Aus dem
Helmholtz-Zentrum München
Institute of Lung Health and Immunity (LHI)

Mesothelial Cell Plasticity and Function: Insights from In Vivo Lineage Tracing, Injury Models, and Human-Derived Cell Studies

Dissertation
zum Erwerb des Doctor of Philosophy (Ph.D.) an der Medizinischen Fakultät der Ludwig-Maximilians-Universität München

vorgelegt von
Yiqun Su

aus
Shandong / China

Jahr
2025

Mit Genehmigung der Medizinischen Fakultät der
Ludwig-Maximilians-Universität München

Erstes Gutachten:	Prof. Dr. Jürgen Behr
Zweites Gutachten:	Dr. Yuval Rinkevich
Drittes Gutachten:	Prof. Dr. Thomas Sitter
Viertes Gutachten:	Prof. Dr. Andreas Ohlmann

Dekan: Prof. Dr. med. Thomas Gudermann

Tag der mündlichen Prüfung: 24.10.2025

Contents

Summary

Mesothelial cells compose a single layer of cobblestone-shaped epithelial cells that cover the surfaces of the peritoneal, pleural, and pericardial body cavities. as well as most internal organs. The mesothelium functions as a critical protective barrier, defending against pathogens and tumor cells through inflammatory and immune responses when injured or exposed to foreign agents. It maintains a smooth, non-adhesive surface to support organ mobility and rapidly repairs itself following damage, typically restoring integrity within days. Disruption of this repair process can lead to pathological changes in the serosal membrane, resulting in adhesions, fibrosis, endometriosis, cancer progression, or metastatic spread.

In this study, we developed inducible CreER knock-in reporter mouse lines, providing a precise tool to trace mesothelial cells in vivo. This system enabled us to analyze the clonal expansion of mesothelial cells at different life stages, from neonatal to adult mice, thereby gaining insights into their distinct proliferative capacities during physiological development and throughout life, at single cell resolution. To further explore mesothelial cell function under pathological conditions, we created a series of disease models, including injury-induced damage, pulmonary fibrosis, and postoperative adhesion models. These models allowed us to systematically study how mesothelial cells respond to and participate in various disease processes, revealing their role in injury response and potential contributions to fibrosis and adhesion formation, at single cell resolutions.

In addition to in vivo models, we have developed an ex vivo tissue culture system as well as a primary human mesothelial cell culture system. These platforms enabled detailed examination of the dynamics of human mesothelial cells in response to various stimuli, linking experimental results to human biological processes. Collectively, these models provide a comprehensive approach to studying mesothelial cell behavior under physiological and pathological conditions, laying the foundation for future studies of therapeutic interventions for mesothelial-related diseases.

Overall, our study established advanced in vivo and ex vivo models to comprehensively investigate mesothelial cell behavior, revealing their roles in development, homeostasis, and disease, and setting the stage for future therapeutic research targeting mesothelial-related pathologies.

1. Introduction

1.1 Overview of Mesothelium

The mesothelium was first characterized in 1827 by Bichat through histological analyses, wherein he documented that serosal cavities are anatomically defined by a continuous squamous epithelium morphologically analogous to lymphatic endothelium. Building on these observations, Minot (1880) conducted systematic embryological investigations, initially designating this tissue as the "epithelium delimiting mammalian mesodermal cavities". This seminal work culminated in his formal proposal of the term "mesothelium" to codify the histological identity of this lining structure [1].

Embryologically, mesothelial progenitors originate from mesoderm between 8-18 post-conception. In human embryogenesis, mesothelial differentiation initiates at approximately embryonic day 14 (E14), through which pluripotent mesenchymal cells undergo a progressive morphological transition from primitive cuboidal/round phenotypes to terminally differentiated squamous epithelia. This cell morphogenesis ultimately establishes the definitive epithelial boundaries of intraembryonic coelomic cavities while concurrently achieving functional maturation of the mesothelial barrier essential for visceral movement [1], the primordium of the 3 major cavities during organogenesis, specific cell populations within developing tissues progressively develop epithelial characteristics, including apicobasal polarity and basement membrane formation. This definitive phenotypic transition establishes the coelomic epithelium, which serves as the embryonic progenitor of postnatal mesothelium [2]. The coelomic epithelium plays a pivotal morphogenetic role in organogenesis through EMT-mediated differentiation. This process generates stromal progenitor populations—including fibroblast precursors and smooth muscle progenitors—that critically contribute to the structural and functional maturation of developing organs [3].

In adult mammals, the mesothelium constitutes a continuous serosal lining that encapsulates both the major body cavities and the external surfaces of their contained viscera, including the pericardium, pleural cavity, and mesentery/peritoneum. Structurally, these membranes consist of two layers: the parietal layer, which lines body cavities, and the visceral layer, which directly covers internal organs [4]. Both layers consist of polarized mesothelial cells attached to a continuous basement membrane, overlying a vascularized

connective tissue stroma that comprises: (1) vascular components (blood/lymphatic capillaries), (2) stromal cellular elements (fibroblasts, mast cells, adipocytes), (3) immunocompetent populations (monocyte-macrophage lineage cells, leukocytes), and (4) neural networks with axonal terminals [5].

The mesothelium was traditionally classified as a simple squamous epithelium fulfilling a passive mechanical role through its lubricious glycocalyx and non-adhesive glycoprotein coating, primarily maintaining the low-friction interface essential for visceral gliding within serosal cavities [6]. However, with the ongoing advancement of research, we are gradually advancing knowledge about the significant role the mesothelium plays in the homeostasis of various diseases. In some cases, when the mesothelium is damaged or subjected to chronic irritation such as by infection, or surgery, its homeostatic balance can be disrupted. This often initiates a cascade of pathological processes, including an inflammatory response and the activation of signaling pathways leading to fibrosis. In severe cases, these disruptions can result in EMT or mesothelial-to-mesenchymal transition (MMT), whereby mesothelial cells differentiate into mesenchymal cells, contributing to ECM deposition and scar formation. Consequently, this process leads to organ adhesions, impaired function, and complications such as chronic inflammation and organ fibrosis [4, 7].

1.2 Functions of Mesothelium and Mesothelial Cell

1.2.1 Protective Barrier and Non-adhesive Surface

The mesothelium functions as a structural and immunological barrier through two mechanisms: (1) intercellular zonula occludens complexes maintaining epithelial integrity against mechanical stress, and (2) production of glycosaminoglycan-rich secretions—principally hyaluronic acid—that polymerize into protective pericellular matrices. These glycocalyx coats envelop apical microvilli, creating both a tribological buffer against shear forces and a biochemical shield limiting pathogenic infiltration.[7]. Hyaluronan exhibits multiple functions in cellular differentiation regulation and postoperative adhesion prophylaxis, while demonstrating inhibitory effects on neoplastic dissemination. Concurrently, mesothelial cells synthesize and release phosphatidylcholine—the principal phospholipid constituent of lamellar bodies—along with surfactant-associated proteins, functioning as boundary

lubricants that minimize interfacial shear stress between apposing serosal membranes [1].

1.2.2 Immunoreactivity or Regulatory Properties

Mesothelial cells actively regulate serosal inflammatory responses through their biosynthetic capacity to produce cytokines, chemokines, growth factors, and extracellular matrix components, coupled with functional expression of intercellular adhesion molecules and antigen-presenting capability [8]. The inflammatory cascade initiates with microbial pathogen-associated molecular patterns (PAMPs) triggering the priming of tissue-resident macrophages and mesothelial cells [9]. This priming phase subsequently progresses to an amplification stage where mesothelial cells assume central importance, becoming activated through exposure to pro-inflammatory mediators—notably TNF-α and IL-1β secreted by peritoneal macrophages [10]. Stimulation of mesothelial cells by pro-inflammatory cytokines, such as TNF-α or IL-1β, triggers the production of IL-8, a potent chemokine that orchestrates leukocyte recruitment and directed migration from the vasculature into the peritoneal cavity [11, 12]. Mesothelial cells constitutively synthesize and display adhesion molecules (ICAM-1, VCAM, PECAM) that serve as critical mediators of leukocyte adhesion and transmigration through the mesothelial monolayer [13, 14]. This process involves several coordinated steps, including the establishment of a chemotactic gradient across the mesothelium, upregulated ICAM-1 expression on mesothelial cells, and selective adhesive interactions between leukocyte integrins and endothelial cell adhesion molecules. Together, these steps enable the precise transmigration of leukocytes across the mesothelial barrier in response to inflammatory cues [15].

Mesothelial-macrophage interactions also play a pivotal role in both the initiation and resolution phases of inflammation. Once the pathogen is eradicated, the resolution of peritoneal inflammation can proceed. The swift and efficient clearance of macrophages is crucial for determining the duration of peritoneal inflammation and is a significant factor in preventing chronic inflammation. In contrast to neutrophils, which are cleared via apoptosis, macrophages are primarily removed through emigration into the draining lymphatic vessels [16]. It has been demonstrated that macrophage emigration from inflamed sites is mediated by VLA-4 and VLA-5, which regulate the

interactions between macrophages and mesothelial cells, and this interaction was RGD-sensitive [17]. Macrophage adhesion to the mesothelium occurs specifically in the region above the draining lymphatic vessels and is dependent on adhesion molecules. Furthermore, the rate of macrophage migration is affected by the level of macrophage activation. Thus, the functional crosstalk between mesothelial cells and macrophages is essential for orchestrating macrophage egress from the peritoneal compartment and driving the resolution phase of serosal inflammation [9].

Mesothelial cells orchestrate inflammatory processes through localized hyaluronan biosynthesis [18], functioning as both radical scavengers and initiators of reparative signaling cascades [19]. Concurrently, these cells modulate inflammatory dynamics in homeostatic and pathological states via cyclooxygenase-mediated metabolism of arachidonic acid, generating prostaglandin/prostacyclin derivatives [11, 20]. These bioactive lipids play critical roles in modulating inflammatory responses and maintaining tissue homeostasis.

1.2.3 Coagulation and Fibrinolysis

Mesothelial cells are central regulators of fibrin turnover dynamics within serosal compartments, maintaining homeostatic balance through plasminogen activator-driven proteolytic activity. This enzymatic process prevents pathological fibrin accumulation secondary to mechanical trauma or microbial invasion while enabling fibrin scaffold dissolution during tissue repair. Dysregulation of this proteolytic pathway culminates in persistent fibrin matrices that promote fibrotic adhesions between apposing serosal membranes through aberrant collagen deposition [21].

Mesothelial cells play a crucial role in maintaining a balance between procoagulant and fibrinolytic activities by producing a range of regulatory factors. They express tissue factor (TF), a potent procoagulant that facilitates the conversion of fibrinogen to fibrin, while also supporting fibrin deposition through the secretion of plasminogen activator inhibitors (PAI), particularly PAI-1 and PAI-2 [22]. The fibrinolytic cascade is mediated through tissue-type plasminogen activator (tPA) and urokinase-type plasminogen activator (uPA), which catalyze the proteolytic conversion of plasminogen to plasmin, initiating enzymatic degradation of fibrin polymers. Mesothelial cells constitute the principal biosynthetic source of tPA within serosal compartments, whereas uPA

expression remains restricted to basal levels under physiological conditions [23]. The biosynthetic output of these mediators is modulated through dual regulatory pathways: pro-inflammatory agonists (LPS, TNF-α, IL-1) and fibrogenic effectors (TGF-β, thrombin), which collectively fine-tune mediator expression levels via NF-κB/Smad-dependent transcriptional mechanism [7].

1.2.4 Mesothelial Regeneration

The mesothelium typically exists in a quiescent state but exhibits significant proliferative plasticity following pathophysiological activation. Within 48 hours post-injury, 30-80% of adjacent mesothelial cells at the injury site and surrounding serosal surfaces synchronously enter S-phase progression. This rapid proliferative response is mediated by paracrine signaling molecules—including cytokines and growth factors—secreted by activated immune cells and injured tissue components within the wound microenvironment [24].

Mesothelial regeneration exhibits distinct pathophysiological characteristics compared to stratified epithelial restitution. Unlike the edge-centric re-epithelialization observed in stratified epithelia, mesothelial repair manifests through pan-mesothelial activation that coordinates cellular mobilization across the entire injured field [25]. This phenomenon facilitates rapid re-establishment of structural continuity independent of lesion dimensions, achieved through unique translocation mechanisms involving both local edge migration and remote cellular recruitment from distant serosal surfaces, followed by targeted repositioning at denuded areas.

Numerous studies have investigated the mechanisms regulating mesothelial regeneration using various types of serosal injuries, including deep lacerations [26], broad abrasions [27], minor linear scarifications [28], drying [29], chemical treatments [30], and heat injuries [24]. These diverse approaches have helped to shed light on the processes involved in mesothelial repair and recovery. These studies have led to the consensus that mesothelial healing begins within 24 hours of injury, marked by the arrival of a population of round cells at the wound site. The mesothelial repair process typically achieves complete functional restoration within 7–10 days, marked by the regeneration of a morphologically and functionally intact monolayer. While the precise cellular origins remain undetermined, proposed mechanisms include centripetal migration of local

mesothelial cells, recruitment of exfoliated cells from adjacent or contralateral serosal surfaces, differentiation of free-floating precursor cells within serosal fluid, macrophage phenotypic conversion, activation of submesothelial mesenchymal progenitors, and potential engraftment of bone marrow-derived circulating stem cells. [31-34].

1.2.5 Mesothelial-to-Mesenchymal Transition

Mesothelial cells undergo mesothelial-to-mesenchymal transition (MMT), a process analogous to epithelial-mesenchymal transition (EMT), to acquire migratory and remodeling capacities. Genetic lineage tracing in murine models demonstrates that during organogenesis, mesothelial-derived cells contribute to vascular smooth muscle development in the gastrointestinal tract, heart, liver, and lungs via MMT, highlighting their critical role in embryonic stromal patterning [35-37]. Mesothelial cells express the transcription factor Wilms tumor-1 (WT-1), which regulates their functional specialization during organogenesis. For example, in pulmonary development, WT-1-positive mesothelial cells migrate into the lung parenchyma and undergo phenotypic transitions to differentiate into bronchial smooth muscle cells, vascular smooth muscle cells, and fibroblasts. This differentiation process is primarily mediated by Sonic Hedgehog (Shh) signaling pathways [38]. In vitro experimental evidence demonstrates that TGF-β1 induces MMT in human mesothelial cells derived from pleural, omental, or mesenteric tissue explants. This transition is characterized by coordinated downregulation of epithelial junctional complexes (E-cadherin, ZO-1), concomitant upregulation of mesenchymal markers (α-smooth muscle actin), and pro-fibrotic extracellular matrix deposition [39, 40]. Complementary studies demonstrate that TGF-β1 and other bioactive mediators—including hepatocyte growth factor (HGF), platelet-derived growth factor (PDGF), and interleukin-1β (IL-1β)—induce transcriptional reprogramming in mesothelial cells. This process activates an evolutionarily conserved EMT-regulatory cassette (SNAI1/2, ZEB1/2, TWIST1) that drives MMT through coordinated epigenetic and post-translational modifications [41-43].

1.2.6 Extracellular Matrix Production

Mesothelial cells maintain serosal membrane homeostasis through strategic biosynthesis of a multifunctional extracellular matrix (ECM) network. Their

synthetic repertoire encompasses structural proteins, adhesive glycoproteins, and hydrophilic proteoglycans that collectively enable mechanical resilience, polarized cellular organization, and damage-responsive remodeling of serosal surfaces [44-47]. Mesothelial cells orchestrate extracellular matrix (ECM) homeostasis through a balanced secretion of proteolytic enzymes (matrix metalloproteinases, MMPs) and their counterregulatory inhibitors (tissue inhibitors of metalloproteinases, TIMPs) [48]. In vitro models reveal that pathological peritoneal effluents from acute peritonitis patients [49], alongside exogenous stimuli such as IL-1β, TNF-α, EGF, PDGF, and TGF-β, significantly enhance ECM biosynthesis in mesothelial cells [50-52].

1.2.7 Key Biomarkers of Mesothelial Cells

Mesothelial cells, which form a monolayer lining the serous cavities (pleura, peritoneum, pericardium), express a variety of key biomarkers that are essential for their identification, functional characterization, and pathological conditions. Among them, podoplanin (PDPN) and protein C receptor (PROCR, also known as EPCR) have emerged as important markers.

PDPN is a transmembrane glycoprotein widely used as a mesothelial marker. PDPN plays a role in cell adhesion, migration, and tissue remodeling. PDPN is highly expressed in normal mesothelial cells and is also present in certain cancers, including malignant mesothelioma. Its role in MMT and tumor progression makes it an important marker in both physiological and pathological settings [53]. Protein C receptor (PROCR/EPCR) is another mesothelial cell marker associated with cell homeostasis and anti-inflammatory signaling. Recent studies have shown that PROCR is involved in regulating mesothelial cell proliferation and differentiation. It has also been associated with stem cell-like properties in mesothelial cells, suggesting a potential role in tissue repair and regeneration [54].

In our lineage-tracing experiments, PDPN served as a crucial marker for visualizing mesothelial cells across multiple organs, including the peritoneum, cecum, and pericardium. Its high specificity enabled precise delineation of mesothelial cell distribution and behavior in various tissues. However, PDPN expression is not exclusive to mesothelial cells. It is also highly expressed in lymphatic endothelial cells, where it contributes to lymphatic vessel function, and in certain fibroblast populations, where it may be involved in tissue

remodeling and fibrosis. Despite this overlapping expression, our ability to distinguish mesothelial cells remained largely unaffected due to the distinct spatial and contextual expression patterns in most tissues.

An exception was the lung, where PDPN is abundantly expressed in alveolar type 1 (AT1) cells, which significantly compromises the ability to track the spatial distribution of mesothelial cells. To address this limitation, we used the PROCR-based lineage-tracing model, which provided a more mesothelial-specific labeling strategy without the confounding influence of PDPN-positive alveolar cells. This approach enabled a more refined investigation of pulmonary mesothelium, facilitating novel insights into its physiological functions and pathological roles.

In addition to PDPN and PROCR, other mesothelial cell markers include mesothelin (MSLN) [57], calretinin [58], WT1 [59], and cytokeratin (CK5/6, CK7, CK8/18) [60], which help identify mesothelial cells and distinguish them from other cell types. These markers are essential for studying mesothelial cell biology, disease progression (e.g., mesothelioma, fibrosis, adhesions), and potential therapeutic targets.

1.3 Pathological Roles of Mesothelial Cells

1.3.1 Postoperative Adhesions

Pathological adhesions manifest as abnormal fusion of serosal surfaces, where adjacent organs or visceral-parietal interfaces form fibrotic connections through excessive deposition of fibrotic matrix components. Recent surgical data indicate that despite significant advancements in microsurgical techniques reducing iatrogenic trauma, clinically relevant adhesions—ranging in severity from chronic pain syndromes to life-threatening bowel obstructions—still occur in 93% of post-laparotomy cases [4]. Pathological adhesions represent a principal etiological factor in chronic pelvic pain syndromes, mechanical intestinal obstruction, and female reproductive dysfunction. The most critical clinical sequela of adhesiogenesis is complete small bowel obstruction, which may clinically present with delayed onset—up to two decades postoperatively—demonstrating associated mortality rates ranging from 3% to 30% in contemporary surgical cohorts [55].

Despite their profound clinical burden, the molecular pathogenesis underlying incipient adhesion formation remains unclear [4]. Previous studies suggest that

pathological adhesion formation arises from dysregulation of physiological serosal repair mechanisms following traumatic injury. Surgical trauma induces mesothelial denudation, triggering an acute-phase response characterized by transient microvascular constriction, endothelial hyperpermeability, and chemokine-mediated recruitment of neutrophils and monocytes to the injury site. This inflammatory milieu activates a fibroproliferative cascade in which mesothelial-derived progenitor cells, activated fibroblasts, and myofibroblasts engage in dysregulated extracellular matrix (ECM) biosynthesis. The resulting fibrinolytic-catabolic imbalance stabilizes provisional fibrinous bridges between apposed tissues, which undergo progressive remodeling via TGF-β-mediated collagen crosslinking, ultimately forming mature fibrotic adhesions [56]. Recent studies highlight mesothelial cells as key regulators in the early stages of post-surgical adhesion formation. Detailed analyses identify cytoskeleton-mediated membrane protrusions and subsequent intercellular fusion between adjacent mesothelial layers as critical drivers initiating adhesion development through aberrant tissue bridging [4]. Studies across multiple adhesion models demonstrate that interactions between mesothelial cells and macrophages critically regulate adhesion development through coordinated molecular signaling [57].

Therapeutic strategies targeting the pathophysiological mechanisms underlying impaired serosal repair—particularly coagulation and inflammatory pathways—have been investigated as potential methods to prevent adhesion formation. Various anti-inflammatory and anticoagulant agents, including corticosteroids, cyclo-oxygenase inhibitors, heparin, and tissue plasminogen activator (tPA), have been administered both systemically and locally to modulate these processes [58-60] The study demonstrated the therapeutic potential of mesothelial cell transplantation in preventing adhesions, with experimental evidence supporting its efficacy as a novel treatment strategy [61, 62]. However, to date, none of these approaches have demonstrated significant effectiveness, and there are no definitive strategies available to reliably prevent the formation of adhesions during surgery [63]. Therefore, elucidating the pathophysiological mechanisms of adhesion development is a key prerequisite for designing innovative therapeutic strategies against adhesions.

1.3.2 Pleural Fibrosis

Pleural fibrosis develops through mechanisms similar to fibrosis in other organs, triggered by conditions such as organized hemorrhagic effusions, infectious processes (tuberculous pleuritis, parapneumonic empyema), asbestos-related pleural injury, and systemic autoimmune diseases.[64]. Clinically, this manifests through two distinct morphological patterns: localized fibrocalcific lesions or extensive diffuse pleural thickening with collagenous matrix deposition.While subpleural fibroblasts are recognized as key drivers of pleural fibrosis, recent studies highlight the critical role of mesothelial cells in coordinating this process. Mesothelial cells contribute to fibrosis through multiple pathways: (1) communication with immune cells via signaling molecules, (2) dysregulation of pro-fibrotic factors like TGF-β and PDGF, and (3) disrupting the balance between blood clotting and clot dissolution.

Although the precise interplay between fibroblasts and mesothelial cells in collagen production remains unclear, current research focuses on their coordinated interactions mediated by inflammatory signals (e.g., IL-1β, TNF-α), growth factors, and reactive molecules. Reactive oxygen species (ROS) play a dual role—directly damaging cells while also activating fibroblasts via Smad/NF-κB signaling pathways. This dual action promotes excessive scar tissue formation and increases production of fibrosis-promoting molecules like TGF-β [65, 66].

1.3.3 Idiopathic Pulmonary Fibrosis

Idiopathic pulmonary fibrosis (IPF) is a chronic, progressive disorder marked by the uncontrolled formation of scar tissue within the lungs. This pathological remodeling disrupts normal lung architecture, leading to irreversible loss of respiratory function and impaired gas exchange. Characterized by persistent fibroblast activation and aberrant extracellular matrix deposition, IPF progressively restricts lung compliance and oxygen diffusion capacity, ultimately resulting in respiratory failure [67]. The pathogenesis of IPF is characterized by progressive fibrotic changes in the lung parenchyma [68]. This progressive and fatal interstitial lung disease presents a median survival period of merely 2–3 years post-diagnosis [69]. Current therapeutic approaches have yet to yield a definitive cure. Phase III clinical trials of antifibrotic agents,

including pirfenidone and nintedanib, have shown efficacy in decelerating disease progression but have not demonstrated the ability to arrest or reverse fibrotic development [70].

While the exact causes of idiopathic pulmonary fibrosis (IPF) remain unclear, current research defines IPF as a progressive scarring disease. Its hallmark features include clusters of activated cells (myofibroblasts) and excessive buildup of scar tissue that disrupts normal lung structure [71, 72]. However, the cellular origin of lung myofibroblasts remains a subject of debate, as evidence suggests that multiple cell types may contribute to the myofibroblast population. Proposed sources include pre-existing peribronchial and perivascular adventitial fibroblasts, alveolar epithelial cells undergoing trans-differentiation (i.e. EMT), bone marrow-derived progenitor cells, tissue-resident mesenchymal cells, and pericytes. These various precursor cells may collectively participate in myofibroblast formation, contributing to the fibrotic remodeling observed in pulmonary diseases [73, 74]. Pleural mesothelial cells (PMCs), constituting the pleural lining, hold critical pathophysiological relevance in IPF given the preferential localization of fibrotic remodeling in subpleural zones. Upon fibrogenic stimulation, PMCs exhibit epithelial-mesenchymal transition characterized by dissolution of apical-basal polarity, disassembly of intercellular junctions, parenchymal invasion, and terminal differentiation into α-SMA-positive myofibroblasts [75-77]. This transformation has been documented in both experimental models and clinical observations of pulmonary fibrosis, underscoring the significant role of PMCs in the fibrotic process of the lung.

1.3.4 Complications of Chronic Peritoneal Dialysis

Peritoneal dialysis (PD) serves as a vital renal replacement modality for end-stage chronic kidney disease (CKD), utilizing the peritoneal membrane as a semipermeable dialysis interface for osmotic-driven toxin/waste product elimination [56]. However, the clinical utility of peritoneal dialysis remains limited by the progressive decline in peritoneal membrane function, which reduces ultrafiltration efficiency and solute clearance capacity during long-term treatment.[78]. Chronic exposure to conventional glucose-based peritoneal dialysis solutions induces progressive peritoneal membrane injury through multiple pathological pathways: sustained inflammatory activation, mesothelial denudation, submesothelial collagen deposition, capillary rarefaction, and

aberrant angiogenesis. These cumulative structural and functional alterations impair osmotic conductance and solute transport capacity, ultimately resulting in peritoneal membrane failure characterized by ultrafiltration insufficiency and progressive dialysis inadequacy. The associated pathological conditions include peritonitis and ultrafiltration failure, which clinically result in extracellular volume overload and increased cardiovascular risk. These factors remain major contributors to technique discontinuation [79, 80].

The bioincompatibility of conventional peritoneal dialysis (PD) solutions and recurrent peritonitis infections drive sustained inflammation and maladaptive repair, leading to progressive structural changes in the peritoneum—mesothelial denudation, aberrant collagen deposition, pathological neovascularization, and vascular hyalinization. These irreversible alterations impair solute clearance and ultrafiltration, ultimately limiting the long-term efficacy of PD [81-83]. Histopathological analysis of peritoneal biopsies from PD patients demonstrates reactive mesothelial transformation marked by hypertrophic mesothelial cells with compromised cellular adhesion and cytodegenerative alterations. These cells exhibit a reduced number of microvilli and show changes in the quantity of endoplasmic reticulum and micropinocytotic vesicles [84].

Chronic exposure of peritoneal mesothelial cells to hyperosmotic glucose dialysate and its reactive carbonyl metabolites impairs cell viability through glucose toxicity-induced apoptosis/necrosis pathways and disrupts homeostatic function through oxidative and carbonyl stress, leading to mesothelial denudation. This pathogenesis is primarily mediated by the coordinated upregulation of proinflammatory mediators, including VEGF and TGF-β1, which are key molecular effectors of peritoneal exacerbations. VEGF promotes neoangiogenesis and disrupts tight junction proteins in mesothelial cells, while TGF-β1 stimulates lymphangiogenesis, EMT, and collagen production, contributing to fibrosis [85, 86]. In addition, the observation that mesothelial cells are shed into the peritoneal cavity during dialysis and may repopulate and repair damaged mesothelium has led to the proposal of mesothelial cell transplantation as a therapeutic strategy to regenerate damaged mesothelium in PD patients [87]. Research indicates that mesothelial cell transplantation is feasible in both animals and humans, and genetically modified mesothelial cells can produce essential proteins to facilitate healing [88, 89]. Emerging therapies targeting TGF-β1 signaling aim to reduce mesothelial

inflammation and prevent fibrosis by inhibiting pathways central to chronic fibro-inflammatory processes [90], reducing mesothelial cell production of fibronectin [91], developing more biocompatible PD solutions, altering PD dwelling times [92], and stimulating fibrinolytic agents [88]. These approaches aim to target mesothelial cells, mitigate the negative effects of chronic peritoneal dialysis on the peritoneum, and improve patient outcomes. However, how these approaches can be routinely applied in patients still requires further investigation. A better understanding of the mechanisms underlying mesothelial cell function is critical to developing novel strategies to prevent disease development.

1.3.5 Cancer-Associated Mesothelial Cells and Mesothelioma

The peritoneum and serous membranes are lined by mesothelial cells, which normally act as a barrier against cancer cell dissemination. However, cancer cells induce mesothelial-mesenchymal transition, transforming these cells into cancer-associated mesothelial cells (CAMs) [93]. CAMs lose their protective function and instead promote tumor metastasis and chemoresistance. They secrete chemokines like IL-8 and CCL2 [94], which enhance cancer cell adhesion, invasion, and neovascularization through pathways such as CXCR1/CXCR2 and p38-MAPK [95, 96]. Additionally, CAMs contribute to extracellular matrix remodeling by upregulating collagen-modifying enzymes (e.g., P4HA, PLOD, LOX) under hypoxic conditions, facilitating cancer cell spread [97].

Malignant mesothelioma is an aggressive tumor that arises from the mesothelial-lined anatomical compartments, with the following major distributions: pleural cavity (65-70%), peritoneal cavity (30%), tunica vaginalis (<1%), and pericardial sac (1-2%) [98]. The most sensitive immunohistochemical markers for identifying mesothelial cells are calretinin (100%), WT1 (94%), and CK5/6 (89%). However, distinguishing between benign and malignant mesothelial cells based solely on immunohistochemical staining can be challenging, as the malignant character of these cells is not always obvious. This diagnostic paradigm has evolved with the introduction of BAP1 (BRCA1-associated protein 1) immunohistochemistry. Loss of BAP1 expression in mesothelial cells is a strong indicator of malignancy and has become a valuable tool in differentiating malignant mesothelioma from reactive mesothelial proliferations [99].

2. Material and Methods

2.1 Mice

The PDPN^{CreERT2} and ProCr^{CreER} mouse line was generated at the Stanford University Research Animal Facility, with Rosa26^{mTmG} and C57BL/6J wild-type mice sourced from Jackson Laboratories or Charles River. The PDPN^{CreERT2} and ProCr^{CreER} mouse lines utilize a tamoxifen-inducible Cre-loxP system for precise gene modification. CreER is expressed in target cells but remains inactive in the cytoplasm. Upon tamoxifen administration, CreER translocates to the nucleus, initiating loxP-mediated recombination to enable conditional gene knockout or activation. When crossed with the Rosa26^{mTmG} reporter, this system allows for visualization of Cre activity. In Rosa26^{mTmG} mice, all cells initially express membrane-bound tdTomato (mT, red fluorescence). Following Cre activation, tdTomato is excised, permitting the expression of membrane-bound GFP (mG, green fluorescence). This red-to-green fluorescence switch precisely marks Cre-expressing cells, facilitating lineage tracing and gene modification studies. Compare to CreER system, CreERT2 is an improved version with lower background activity and higher sensitivity to tamoxifen. This makes CreERT2 more precise and reliable for conditional gene recombination

All animals were maintained in the Helmholtz Central Animal Facility under standard environmental conditions (controlled temperature and humidity) with a 12-hour light/dark cycle and *ad libitum* access to food and water. All experimental protocols were conducted in compliance with institutional guidelines and ethically approved by the Upper Bavarian State Government Animal Ethics Committee. (TVA Nos. ROB-55.2-2532.Vet_02-18-62, ROB-55.2-2532.Vet_02-20-216, ROB-55.2-2532.Vet_02-17-97, and ROB-55.2-2532.Vet_02-19-101).

2.2 Mice Genotyping

Genotyping was performed to identify mice carrying the 190-bp PDPN^{CreERT} allele. Genomic DNA was isolated from ear punch biopsies using the Quick Extract™ DNA Extraction Solution according to the manufacturer's protocol. For PCR amplification, 1 µL of extracted DNA was combined with 19 µL of reaction mixture prepared with GoTaq™ Green Master Mix. Each reaction contained 1X GoTaq enzyme mix, 0.5 µM forward primer (1318flp-YRI2: 5′-GAT GGG GAA

CAG GGC AAG TTG G C-3′, Sigma), and 0.5 µM reverse primer (1320flp-YRI2: 5′-GGC TCT ACT TCA TCG CAT TCC TTG C-3′, Sigma). The thermal cycling conditions were set as follows: an initial denaturation at 94°C for 5 minutes, followed by 35 cycles of amplification, each consisting of denaturation at 94°C for 30 seconds, primer annealing at 65°C for 30 seconds, and strand extension at 68°C for 1 minute. Reactions concluded with terminal extension at 68°C for 10 min, followed by thermal cycler stabilization at 4°C Each experiment included negative controls and positive controls. PCRs were conducted on a ProFlex PCR System, and the amplicons were analyzed via gel electrophoresis.

For the ProCr^{CreER} mouse, a 1 µl DNA extract was added to each 19 µl PCR reaction. The reaction mixture was prepared using the GoTaq Green Master Mix kit (Promega, Cat# M7123), containing 1X GoTaq Green Master Mix.0.5 µM forward primer “Cre-FW” (5′-GCG GTC TGG CAG TAA AAA CTA TC-3′; Sigma), and 0.5 µM reverse primer “Cre-RV” (5′-GTG AAA CAG CAT TGC TGT CAC TT-3′; Sigma). The thermal cycling parameters were programmed as follows: initial template denaturation at 94°C for 5 min, followed by 24 amplification cycles consisting of three sequential stages template denaturation (94°C, 30 sec), primer annealing (59°C, 30 sec), and strand extension (72°C, 1 min) - concluding with final extension at 72°C for 10 min, followed by infinite hold at 4°C. Each experiment included negative controls and positive controls. PCR reactions were performed using the Life Technologies ProFlex PCR System, and the products were analyzed via gel electrophoresis.

2.3 Tamoxifen Preparation

All experimental procedures utilized bioactive 4-hydroxytamoxifen (4-OHT), the active metabolite of tamoxifen. Initial preparations began by dissolving 50 mg of lyophilized 4-OHT powder in 3 mL of absolute ethanol (100%) through vigorous vortex mixing (2,000 rpm) for 5–7 minutes until complete dissolution. The homogeneous ethanolic solution was then aliquoted and subjected to solvent evaporation using a speed vacuum concentrator operated at 45°C for 2–4 hours with tube lids open to facilitate ethanol removal. The dried 4-OHT residues were stored at –80°C under inert atmosphere.

For experimental application, each aliquot was reconstituted in 500 µL of corn oil (pharmacologically inert vehicle) and homogenized via sequential sonication.

This involved four consecutive sonication runs (10 minutes per run) under pulsed conditions (30 seconds ON / 30 seconds OFF per cycle at 40 kHz frequency) to ensure uniform dispersion. The final 4-OHT/corn oil solutions were protected from light and stored at –20°C.

2.4 Clonal Tracing of Mesothelial Cells

To trace clonal expansion in mesothelial cells, $PDPN^{CreERT2}$ $R26^{mTmG}$ mice were injected intraperitoneally with 1mg of 4-hydroxytamoxifen to label single mesothelial cells. The injections were administered to adult mice aged 6–7 weeks, with initial tracing observed 7 days post-injection. Organs, including the peritoneal wall, large lobe of the liver, cecum, lung, and heart, were then collected at specified time points of 7 days, 3 months, 6 months, and 1 year to monitor long-term clonal dynamics.

For neonatal tracing, P0 pups received a single dose of 4-OH Tam injections, with organ collection at days 2, 7, and 30.

2.5 Mouse Adhesion Model

To establish the mouse adhesion model, anesthesia was induced via intraperitoneal administration of a triple anesthetic cocktail (medetomidine 500 μg/kg, midazolam 5 mg/kg, fentanyl 50 μg/kg), with anesthetic depth verified through serial assessment of pedal withdrawal reflexes. Ocular protection was ensured through application of dexpanthenol-containing ophthalmic ointment, followed by abdominal depilation and aseptic preparation using 10% povidone-iodine solution. Subjects were positioned in dorsal recumbency on a temperature-regulated heating platform (37°C) to maintain normothermia.

Aseptic ventral midline laparotomy was performed by making a 1-2 cm incision through sequential layers of the integument and peritoneum under sterile conditions. Surgical exposure of the operative field was achieved by positioning four stainless steel retractor hooks equidistantly along the wound margins, which were stabilized using a magnet-anchored self-retaining retractor system to maintain consistent tissue visualization. Throughout the procedure, intraoperative hydration was ensured via intermittent subcutaneous administration of 0.9% saline solution to counteract fluid loss and maintain hemodynamic stability.

Mechanical abrasion of the peritoneal mesothelium and adjacent cecal serosa was performed using a sterile nylon-bristled surgical brush (3 mm diameter) to establish standardized serosal injury. The denuded peritoneal surface was approximated with interrupted 4-0 silk sutures in a tension-free pattern. To potentiate the fibroinflammatory response, sterile medical-grade talcum powder (magnesium silicate hydrate) was topically applied as a pro-inflammatory irritant using calcium alginate-tipped applicators.

Preemptive analgesia was achieved through intraperitoneal administration of buprenorphine HCl (0.1 mg/kg) prior to fascial closure. Sustained postoperative analgesia was maintained via metamizole sodium (1.25 mg/mL) supplementation in autoclaved drinking water ad libitum, with daily consumption monitoring to ensure therapeutic plasma concentrations.

2.6 Bleomycin-Induced Lung Fibrosis Model

Mice were anesthetized by intraperitoneal injection of a mixture containing medetomidine (500 μg/kg), midazolam (5 mg/kg), and fentanyl (50 μg/kg). The depth of anesthesia was monitored using the toe reflex. To prevent dehydration, the eyes of the mice were protected with Bepanthen ointment. To induce lung inflammation and fibrosis, a single dose of bleomycin sulfate in PBS was instilled intratracheally at a concentration of 2 U/kg. Control mice received a single dose of PBS by the same route. Table 1 outlines the volume of bleomycin and PBS adjusted according to the weight of the mice (ranging from 20 to 33 g) to ensure a consistent final instillation volume of 80 μl for all subjects. To facilitate recovery from anesthesia, an antagonist combination of atipamezole (2.5 mg/kg), flumazenil (500 μg/kg), and naloxone (1200 μg/kg) was injected subcutaneously to reverse the effects of the MMF anesthetic mixture.

Table 1 Dosage of bleomycin

Weight (g)	Bleomycin (μl)	PBS (μl)	Total Volume (μl)
20	2.67	77.33	80
21	2.80	77.20	80
22	2.93	77.07	80
23	3.07	76.93	80
24	3.20	76.80	80

25	**3.33**	**76.67**	**80**
26	**3.47**	**76.53**	**80**
27	**3.60**	**76.40**	**80**
28	**3.73**	**76.27**	**80**
29	**3.87**	**76.13**	**80**
30	**4.00**	**76.00**	**80**
31	**4.13**	**75.87**	**80**
32	**4.27**	**75.73**	**80**
33	**4.40**	**75.60**	**80**

2.7 Tissue Collection and 3D Staining

After excision, tissues were fixed in 2% PFA and PBS solution at 4°C overnight. The next day, fixed tissues were rinsed three times with PBS and then transferred to PBS-GT solution (PBS containing 0.2% gelatin, 0.5% Triton-X, and 0.01% thimerosal) and stored at 4°C.

Samples in PBS-GT were incubated with primary antibodies (1:500 dilution) for 36 hours at room temperature under gentle agitation, followed by overnight PBS-GT washes. Secondary antibodies in PBS-GT were then applied under identical incubation conditions (36 hours, RT, shaking). Post-secondary antibody treatment, tissues underwent sequential PBS-GT washes, including a final overnight wash at RT. Processed samples were stored in PBS prior to imaging.

2.8 Tissue Sections and Immunofluorescence Staining

Tissue samples were embedded in O.C.T. Compound and sectioned using a Hyrax C5 cryostat. Sections were stored at -20°C until staining. The immunofluorescence protocol included fixation in cold acetone for 3 minutes, followed by three PBS washes (5 minutes each), blocking with 5% BSA in PBS for 1 hour at room temperature, overnight incubation with primary antibodies (diluted in 1% BSA/PBS) at 4°C, three extensive PBS washes (20 minutes each), incubation with secondary antibodies (diluted in 1% BSA/PBS) for 2 hours at room temperature in the dark, final PBS washes, and mounting with Fluoromount-G™ containing DAPI.

2.9 Masson Trichrome Staining

Tissue sections were fixed in ice-cold acetone (-20°C) for 10 minutes, air-dried for 5 minutes, and rehydrated in deionized water for 2 minutes. Slides were then incubated in preheated Bouin's solution at 56°C for 15 minutes to enhance staining, followed by thorough rinsing under running tap water. Nuclear structures were stained with Weigert's Iron Hematoxylin (3 minutes, room temperature, while cytoplasmic components were highlighted using Biebrich Scarlet-Acid Fuchsin (5 minutes, RT). Collagen differentiation was achieved by immersion in a phosphotungstic/phosphomolybdic acid working solution (45 mL phosphotungstic acid + 45 mL phosphomolybdic acid + 90 mL deionized water) for 5 minutes at RT. Sections were counterstained with Aniline Blue (10 minutes, RT) to visualize connective tissue, stabilized in 1% acetic acid (2 minutes), and rinsed with distilled water. Dehydration was performed through graded ethanol series (80% ethanol → 100% ethanol, 5 minutes each). Tissue clearing was accomplished using Roti-Histol, followed by permanent mounting with Roti-Histokitt. This protocol achieves distinct nuclear (dark brown), cytoplasmic (red), and collagenous (blue) differentiation, preserving histological architecture for morphological analysis.

2.10 2D and 3D Imaging of Samples

High-resolution imaging was performed using confocal (Zeiss LSM710) and epifluorescence (Zeiss AxioImager2) microscopy. Whole-mount tissues were visualized in 3D by mounting in 35-mm glass-bottom dishes and imaging with the LSM710 confocal system, while trichrome-stained sections were analyzed via brightfield microscopy (AxioImager2) and fluorescently labeled samples via LSM710 confocal imaging.

2.11 Image Analysis and Statistic

Image processing and quantitative analyses were conducted using ImageJ (v2.1.0), followed by statistical evaluations in GraphPad Prism (v9.4.1). Comparisons between two experimental groups were analyzed via Student's t-test, while multi-group comparisons employed one-way ANOVA with post hoc

multiple comparisons against control groups to assess statistical significance.

2.12 Cell Segmentation Analysis

Images were processed and analyzed using ImageJ software (version 2.1.0), with the analysis automated via a custom script designed to batch process “.jpg” images within a specified directory. Initially, images were opened, and the global scale was established (Analyze > Set Scale). The images were then converted to 8-bit grayscale (Image > Type > 8-bit). MorphoLibJ was utilized for image segmentation (MorphoLibJ > Segmentation > Morphological Segmentation). The input image was designated as the "border image," followed by executing Watershed Segmentation, with a tolerance set to 65. Advanced options were subsequently selected, setting "Connectivity" to 8, and the results were displayed as “Catchment basins” to create the segmented image. Finally, the segmented regions were analyzed (MorphoLibJ > Analyze > Analyze Regions), where parameters such as “Area,” “Circularity,” and “Max. Feret Diameter” were selected for evaluation.

2.13 Human Tissue Collection and Primary Mesothelial Cell Isolation

Human adhesion tissues and greater omentum samples were collected during abdominal surgeries at the Department of Surgery, Klinikum rechts der Isar, in accordance with ethical approval granted by the Institutional Review Board of TUM’s Faculty of Medicine (Ethics No. 95/22 S-KK). All participants provided written informed consent prior to tissue collection and study inclusion.

Human greater omentum specimens were collected in Hank’s Balanced Salt Solution (HBSS) and processed aseptically. Tissues were minced into 1–2 mm^3 fragments, washed in PBS to remove blood components, and subjected to enzymatic dissociation in 0.05% (w/v) trypsin-EDTA solution at 37°C for 5–7 minutes under constant agitation (120 rpm). Trypsin activity was neutralized by adding an equal volume of RPMI-1640 medium supplemented with 10% FBS . The cell suspension was centrifuged (250 ×g, 5 min, 4°C), pelleted cells were resuspended in complete growth medium (Medium 199 containing 10% FBS,

50 U/mL penicillin-streptomycin, 16 ng/mL insulin-transferrin-selenium (ITS), 400 nM hydrocortisone, and 3.3 nM epidermal growth factor (EGF), and seeded into 3.5 cm tissue culture-treated dishes. Culture medium was replaced every 48 hours until 80% confluency.

2.14 Immunostaining of Cells

Cells grown in 8-well Lab-Tek chamber slides were fixed with 4% PFA in PBS for 15 minutes, washed three times with PBS, and permeabilized with 0.1% Triton X-100 in PBS for 15 minutes . Blocking was performed using 5% donkey serum in PBS (30 minutes). Primary antibodies diluted in PBS were applied for 1 hour at room temperature, followed by three PBS washes. Cells were then incubated with fluorescently labeled secondary antibodies and 0.5 mg/mL DAPI (nuclear stain) for 1 hour, washed three times with PBS, and stored at 4°C until imaging.

2.15 ER-Hoxb8 Cell Culture and Differentiation

The ER-Hoxb8 system enables scalable production and genetic manipulation of macrophages by conditionally immortalizing murine bone marrow-derived myeloid progenitors. This method utilizes estrogen-regulated Hoxb8 overexpression to block differentiation while promoting progenitor cell expansion. Transduction with ER-Hoxb8 retrovirus confers estrogen-dependent immortalization, allowing indefinite culture in estrogen-supplemented media. Upon estrogen removal, progenitors synchronously differentiate into functional macrophages. This platform supports high-yield generation of genetically editable macrophages and bipotential lymphoid-myeloid progenitors, facilitating studies of innate immunity and hematopoietic development [100].

Cells were obtained by the Harvard Stem Cell Institute at Harvard Medical School and maintained in a complete medium consisting of RPMI 1640 supplemented with 10% FBS, 50 μM 2-mercaptoethanol, 1 μM β-estradiol, and 5% GM-CSF-conditioned medium. The GM-CSF-conditioned medium was derived from the supernatant of B16-GM-CSF cells, which constitutively express murine GM-CSF and were also obtained from the Harvard Stem Cell Institute.

To induce macrophage differentiation, ER-Hoxb8 cells were harvested and subjected to two washes with sterile PBS to thoroughly remove residual GM-

CSF and β-estradiol. Cells were subsequently seeded into P6-well culture plates at a density of 1×10^5 cells/well and maintained in RPMI-1640 complete medium containing 20 ng/mL recombinant human macrophage colony-stimulating factor (M-CSF). Cultures were incubated for 7 days at 37°C under 5% CO_2 with medium replacement every 48 hours to ensure sustained M-CSF activity.

For polarization towards M1 or M2 macrophages, ER-Hoxb8 macrophages (5×10^5 cells/well) were incubated in a complete RPMI 1640 medium supplemented with LPS (1 μg/mL) and γ-IFN (20 ng/mL) for M1 polarization or IL-4(20 ng/mL) for M2 polarization, respectively, as previously described. After 48 hours, the polarized macrophages were harvested for phenotypic analysis using the following markers: APC anti-mouse F4/80, PerCP/Cyanine5.5 anti-mouse CD80, and PE/Cyanine7 anti-mouse CD206 via flow cytometry, with dead cells excluded by Sytox Green.

2.16 Tissue-Cell Co-Culture Assay

C57BL/6J male and female mice aged 6-12 weeks were used for peritoneal tissue collection. Peritoneal tissues of uniform dimensions (6 mm) were obtained using biopsy punches. Each tissue piece was placed in a 12-well tissue culture plate and co-cultured with 1×10^5 ER-Hoxb8-derived macrophages in RPMI medium supplemented with 20% FBS for 24 to 48 hours.

2.17 3D multiphoton imaging of samples

Following fixation, explants underwent three 1-hour PBS washes and were embedded in NuSieve™ GTG agarose within 35 mm dishes. Three-dimensional imaging was performed on a Leica SP8 upright multiphoton microscope (DM6 stand, Scientifica stage) using 966 nm excitation wavelength. Second harmonic generation (SHG) signals were captured at 483 nm, while fluorescence emissions were detected via bandpass filters (orange: 585 nm; far red: 624 nm; green: 525 nm). Stitched tile scans were processed in LAS X software and reconstructed in Imaris for 3D visualization, with contrast/brightness optimized post-acquisition.

2.18 ScRNA-seq data analysis

All the analyses were performed using the python toolkit Scanpy and complementary tools under its ecosystem. Publicly available scRNAseq matrices from mouse pleura-, pericardium-, and peritoneum-related organs at different developmental stages were obtained from the GEO repository (table). To decrease platform-based effects, only samples generated with the 10X chromium chemistries were included. Matrices of individual samples were quality checked (doublet-detection with Scrublet), filtered (cells with minimum 100 genes), and concatenated. Outlier cells from the same study/batch (collection" with 3 median absolute deviations or above 8 or 10 percentage of mitochondrial (Mt-) or hemoglobin (Hb) genes respectively were also filtered. Same for cells with 5 median absolute deviations from total counts, genes by counts, and counts in top 20 genes metrics as recommended in the www.sc-best-practices.org book. Furthermore, outliers with 5 median absolute deviations or above 50 percentage of ribosomal genes were also filtered. Individual batches ('collection') objects were then concatenated and their raw counts normalized and log-transformed. The UMAP algorithm was the preferred dimensional reduction method together with the "Harmonipy." graph-based batch effect correction. For each atlas, major cell types were annotated based on the expression of classical lineage markers. Cell cycle phases annotation was performed with the in-built cell cycle gene score function in Scanpy. The Mouse Organogenesis Spatiotemporal Transcriptomic Atlas (MOSTA) was obtained from the STomicsDB (db.cngb.org/stomics/mosta) and analysed with Squidpy. Top 10 ranked marker genes for mesothelial cells across the 3 scRNAseq atlases were scored in the MOSTA datasets to reveal the mesothelial cells-containing regions within the mouse embryo.

3 Results

3.1 Mesothelial Cells Proliferate Rapidly During Early Organ Development

To enable single-cell labeling of mesothelial cells on organ surfaces, an optimal concentration of 4-OH tamoxifen was given via i.p. injection. This single-cell analysis is essential for investigating clonal expansions that originate from labeled cells over time.

Firstly, an optimized single dose of 4-hydroxytamoxifen was administered to neonatal PDPN^{CreERT2} mice to ensure that the majority of labeled mesothelial cells were in a single-cell state (**Fig 1A**). To investigate changes in mesothelial cells during organ growth, we collected various organs on day 2, day 7, and day 30 post-administration and analyzed the proportion of organ surface clones containing more than 4 cells (**Fig 1B**). **Figures 1C–1F** show mesothelial cell lineage tracing across the lung, liver, peritoneum, and heart, visualized through GFP fluorescence (green) and PDPN immunofluorescence staining (magenta). Although the cecum is an organ covered by mesothelium and closely related to this study, it was excluded due to the incomplete development of neonatal mice, making it challenging to define the cecum rigorously. Quantitative analysis of the data indicates the proportion of clones with four or more cells during postnatal development. The results demonstrate that mesothelial cells undergo rapid proliferation during early organ development, as reflected by a significant increase in clone size by day 7. This suggests that mesothelial cells may play an important role in supporting organ growth and development. However, by day 30, no substantial increase in clonal size is observed compared to day 7, indicating a reduction in mesothelial cell proliferation as the organs approach maturation.

Additionally, our analysis revealed heterogeneity in mesothelial cell clone sizes during early development (data not shown), with the presence of single cells, small clones (≤4 cells), and large clones observed concurrently on the organ surfaces. This suggests that mesothelial cells may exhibit intrinsic variability, potentially reflecting differential cell states or the occurrence of dynamic processes such as cell differentiation, apoptosis, or selective survival. Such

variability could indicate a complex regulation of mesothelial cell behavior during development. Overall, these findings highlight the dynamic nature of mesothelial cell proliferation, characterized by a rapid increase in activity during early developmental stages, which likely supports organ growth and morphogenesis.

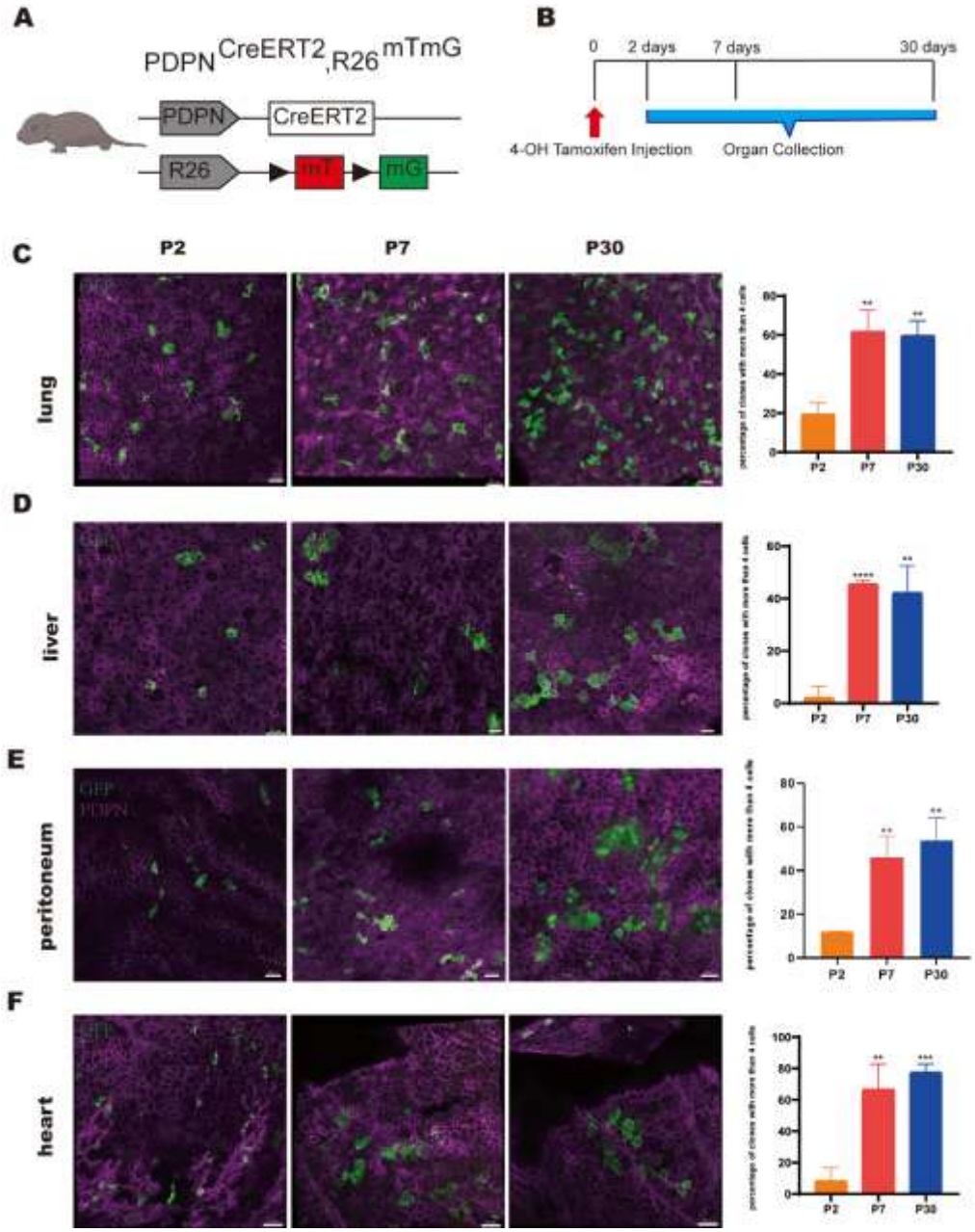

Figure 1: Clonal Formation of Mesothelial Cells on Organ Surfaces in Neonatal Mice. (A) Overview of the experimental setup of the PDPN^{CreERT2} mouse. (B) Time point of Tamoxifen injection and organ collection. (C) Representative images and statistics of mesothelial cell clones with over four cells on the lung surface. (D) Representative images and statistics of mesothelial cell clones with over four cells on the liver surface. (E) Representative images and statistics of mesothelial

cell clones with over four cells on the peritoneum. (F) Representative images and statistics of mesothelial cell clones with over four cells on the heart surface. Scale bar=50μm. n = 3 biological repeats **p ≤ 0.01; ***p≤ 0.001 two-tailed t-test.

3.2 Mesothelial Cells Exhibit Limited Proliferative Capacity During Adult homeostasis

To evaluate the in vivo proliferative potential of mesothelial cells under adult homeostatic conditions, tamoxifen-induced genetic recombination was performed using $PDPN^{CreERT2}$ transgenic mouse models (**Fig 2A**). Mice aged 6–7 weeks received a single intraperitoneal injection of 4-hydroxytamoxifen, and organs were collected at day 7, 3 months, 6 months, and 1 year time points. (**Fig 2B**). In this study, we systematically assessed the proliferative capacity and clonal formation of mesothelial cells across various organs in adult mice, including the lung, liver, cecum, peritoneum, and heart, using mesothelial cell lineage tracing. **Figures 2C–2G** illustrate the tracing of mesothelial cell clones, visualized via GFP fluorescence (green) and PDPN immunofluorescence (magenta). Unlike the robust clonal formation and proliferative activity observed in neonatal mesothelial cells, adult mesothelial cells exhibited minimal clonogenic potential by day 7, suggesting a diminished proliferative capacity during adulthood.

At 3 months, a significant increase in the proportion of cells within clones was observed exclusively in the cecum, indicating that mesothelial cells in this organ may exhibit a more pronounced proliferative response compared to other organs (**Fig 2E**). By 6 months, clonal expansion became evident on the lung surface, with a notable increase in clone formation, suggesting that mesothelial cells in the lung may undergo a delayed proliferative phase compared to the cecum (**Fig 2C**). In contrast, significant clonal formation on the heart and liver surfaces was not observed until 1 year, indicating that mesothelial cells in these organs exhibit a relatively slow or later phase of clonal expansion (**Fig 2D 2G**). Remarkably, no significant clonogenesis was detected in the peritoneum throughout the entire one-year observation period, pointing to a distinct regulatory mechanism that restricts or suppresses mesothelial cell proliferation during adulthood (**Fig 2F**). This lack of clonal activity in the peritoneum contrasts sharply with the proliferative responses seen in other organs, further

emphasizing organ-specific regulation of mesothelial cell turnover.

Together, these findings underscore the complex, organ-specific, and age-dependent nature of mesothelial cell proliferation. While neonatal mesothelial cells demonstrate significant clonal activity, adult mesothelial cells exhibit a more restricted proliferative potential, with distinct temporal patterns of clonal expansion across different organs. These results contribute to our understanding of mesothelial cell dynamics in adult organs and highlight the role of mesothelial cells in organ-specific homeostasis maintenance.

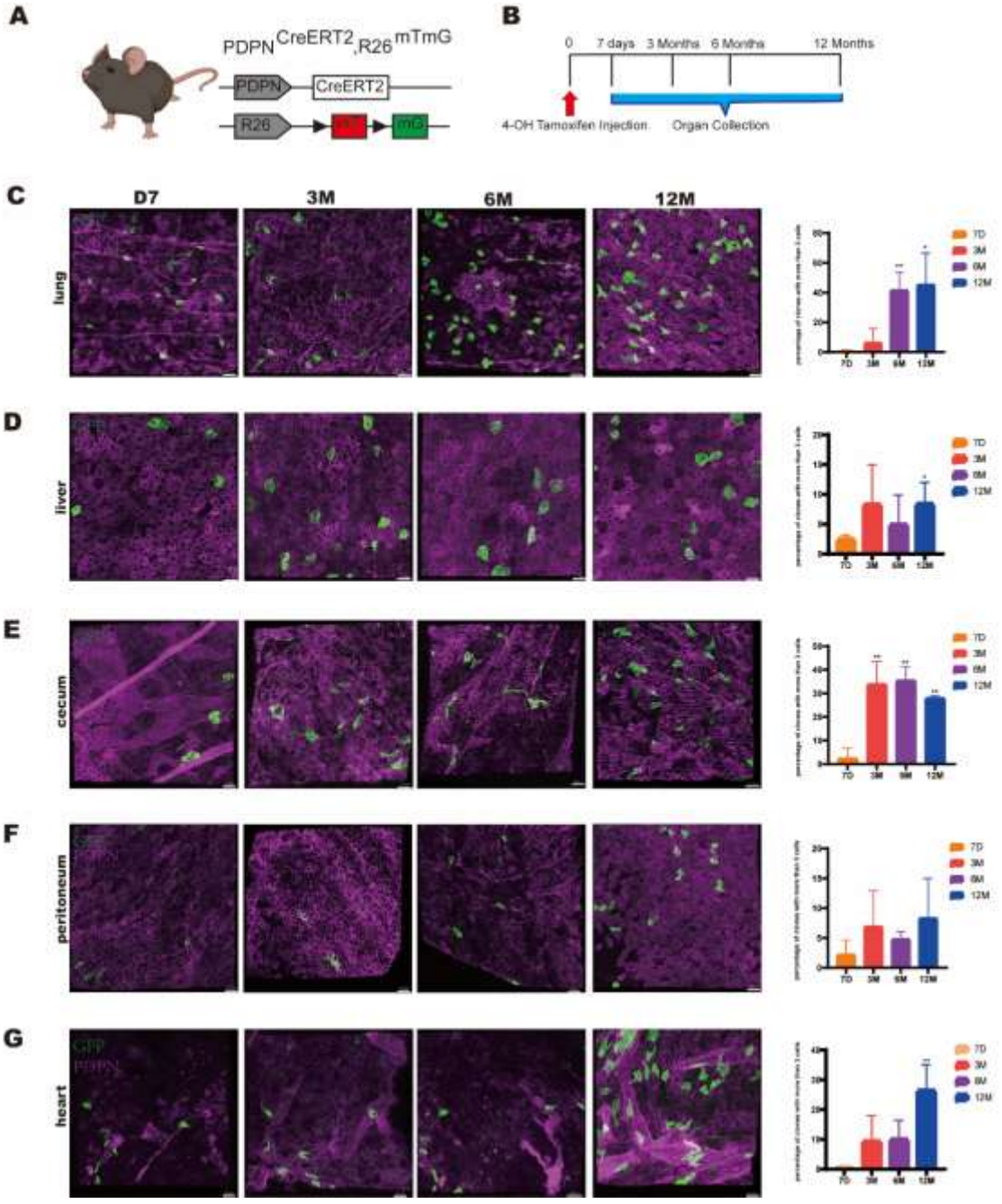

Figure 2: Clonal Formation of Mesothelial Cells on Organ Surfaces in Adult Mice. (A) Overview of the experimental setup of the transgenic mouse. (B) Time points of Tamoxifen injection and organ collection. (C) Representative images and statistics of mesothelial cell clones with over three cells on the lung surface. (D) Representative images and statistics of mesothelial cell clones with over three cells on the liver surface. (E) Representative images and statistics of mesothelial cell clones with over three cells on the cecum surface. (F) Representative images and statistics of mesothelial cell clones with over three cells on the peritoneum surface. (G) Representative images and statistics of mesothelial cell clones with over three cells on the heart surface. GFP-labeled mesothelial cells (green), with PDPN immunofluorescence (magenta) Scale bar=50μm. n = 3 biological repeats. *p ≤ 0.05; **p ≤ 0.01; ***p≤ 0.001; two-tailed t-test.

3.3 Mesothelial Cell Dynamics in Organ Development

To investigate the mechanisms driving clonal emergence and regeneration of mesothelium, we integrated publicly available scRNA-seq datasets of pericardium (**Fig 3A right**), pleura (**Fig 3B right**), and peritoneum (**Fig 3C right**). This integrated dataset comprised 932,063 high-quality cells from 252 samples across 60 datasets. Mesothelial cells in each dataset were identified based on the co-expression of mesothelial markers such as WT1, MSLN, C3, Gpm6a, PROCR, PDPN, and Upk3b (**Fig 3A-C left**). Consistent with the mesothelium forming a single epithelial layer on organ surfaces, a distinct mesothelial cell cluster was identified. These accounted for 4.12% of total cells in the heart (14,428 out of 350,458), 0.62% in the lungs (1,750 out of 283,964), and 1.82% in the peritoneum (5,417 out of 297,641) (**Fig 4A-C Middle**).

Spatial transcriptomics is a cutting-edge technique enabling the precise localization of gene expression within tissue architecture. The MOSTA (Mesothelium Spatial Transcriptomics Atlas) framework extends this approach by providing spatially resolved transcriptomic profiles of mesothelial cells across different organs. It combines spatial context with high-resolution molecular data, offering a detailed view of mesothelial cell heterogeneity, spatial organization, and interactions with the surrounding microenvironment. Through MOSTA analysis of mesothelial cells from embryonic day 9.5 (E9.5) to E16.5, we observed dynamic gene expression changes during distinct stages of

embryonic development and spatial distribution changes of mesothelial cells during embryonic development (**Fig 3D**). These findings further support the notion that mesothelial cells likely play a critical role in organ development during the embryonic period. The observed transcriptional shifts highlight their involvement in processes such as tissue morphogenesis, cell proliferation, and differentiation, underscoring their essential contribution to the proper formation and maturation of organs during this pivotal developmental window.

By analyzing three developmental datasets that represented different stages of organ growth to understand the dynamics of mesothelial cell proliferation over time. In the early stages of development, a substantial proportion of mesothelial cells were found in the S phase and G2/M phases of the cell cycle, indicating active DNA replication and mitosis. This observation aligns with our clonal analysis, which highlighted a high proliferative capacity during these initial stages of organ growth.

In contrast, as development progressed, the proportion of actively dividing mesothelial cells decreased significantly. By the later stages, most mesothelial cells were predominantly in the G1 phase of the cell cycle, reflecting a shift to a quiescent or resting state. This temporal change underscores the transition from a highly proliferative state during early organ formation to a more stable and homeostatic state in adulthood, where mesothelial cell proliferation becomes more restricted. These findings provide critical insights into the developmental regulation of mesothelial cell dynamics and their role in organ maturation (**Fig 4A-C left**).

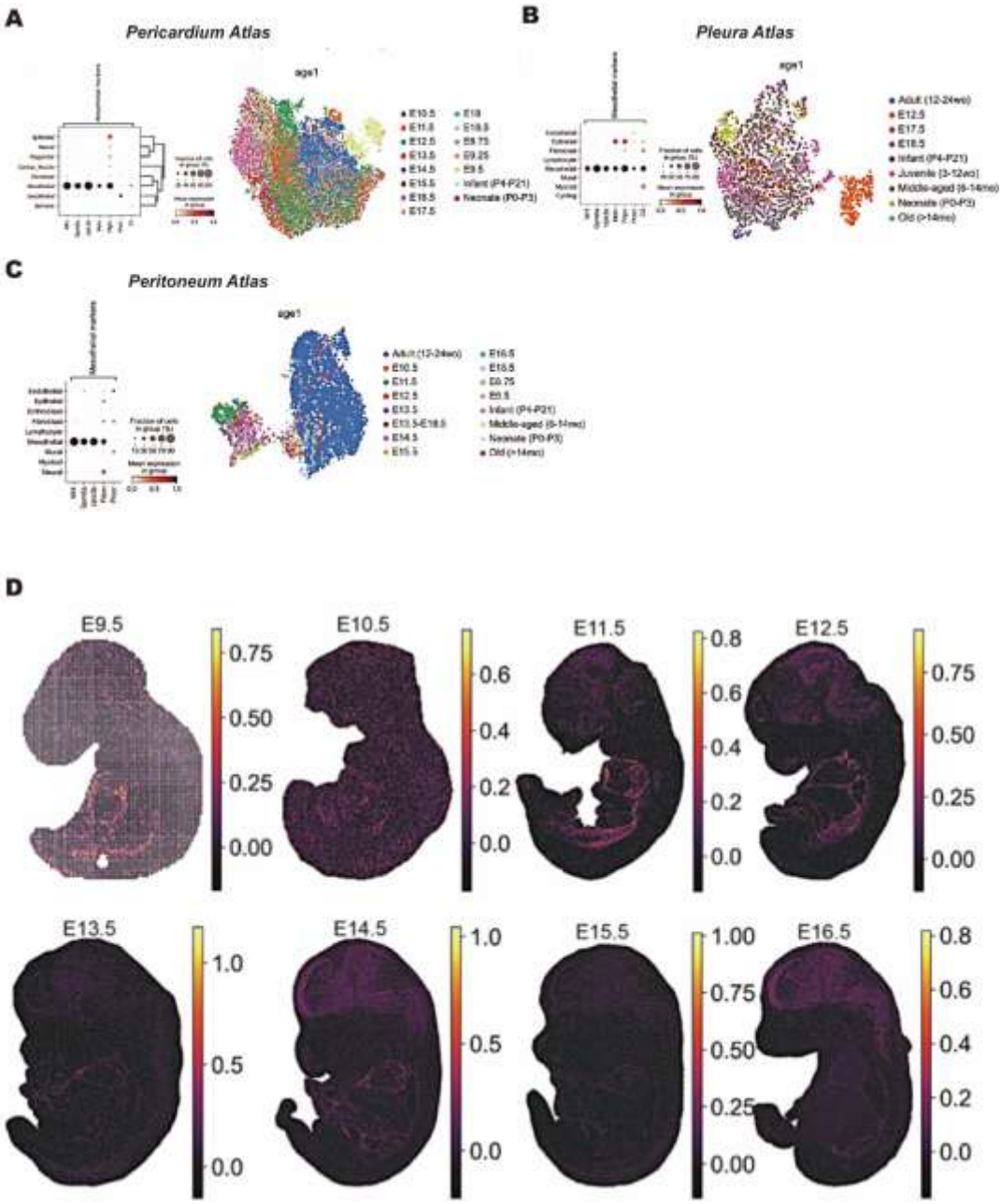

Figure 3: Peritoneum, Pleural, and Pericardium mesothelial cell single cell analysis during development. (A-C) UMAP plots of mesothelial cells across different organ atlases. For each organ—pericardium (A), pleura (B), and peritoneum (C)—the left panels display identified mesothelial cells, while the right panels show mesothelial cells at different stages of development. (D) Spatial transcriptomics (MOSTA). Combined expression score of Msln, Wt1, Upk3b, Gpm6a, Pdpn & Procr.

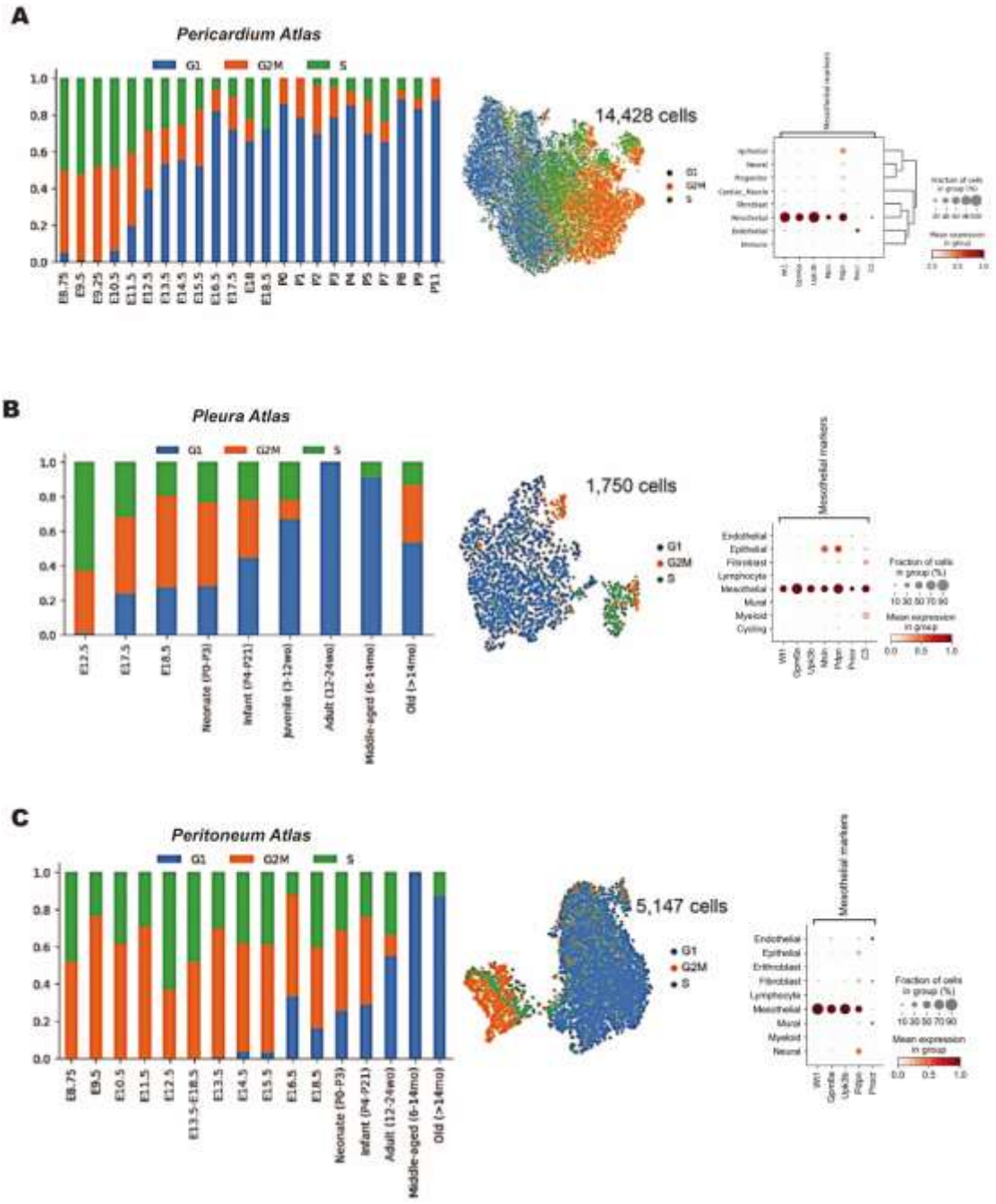

Figure 4: Distribution of mesothelial cells across cell cycle phases at different embryonic stages and development. (A) Pericardium Atlas (Development): Identification and classification of 14428 mesothelial cells based on their cell cycle stages. (B) Pleura Atlas (Development): Identification and classification of 1750 mesothelial cells based on their cell cycle stages. (C) Peritoneum Atlas (Development): Identification and classification of 5147 mesothelial cells based on their cell cycle stages.

3.4 Diverse Behaviors of Mesothelial Cells in Bleomycin-Induced Idiopathic Pulmonary Fibrosis Model

3.4.1 Excessive Proliferation of Mesothelial Cells on the Lung Surface

Interstitial lung diseases (ILDs) comprise various disorders causing chronic inflammation and fibrosis, leading to impaired gas exchange. About 50% of cases are idiopathic, with idiopathic pulmonary fibrosis (IPF) as a distinct subtype marked by progressive scarring. While its pathogenesis is unclear, IPF shares fibrotic mechanisms with systemic fibrosis, including dysregulated repair, excessive ECM deposition, and impaired injury resolution.

In IPF, myofibroblasts, identified by α-SMA and vimentin expression, are recognized as key effector cells responsible for ECM deposition. However, the cellular origin of lung myofibroblasts remains debated, with evidence suggesting that multiple cell types may contribute as precursors. To investigate whether mesothelial cells undergo proliferation, differentiation, or spatial distribution changes during IPF, we utilized a lineage-tracing model. Notably, while PDPN effectively and specifically labels mesothelial cells in most organs, its broad expression in AT1 cells makes it unsuitable for lung studies, as it obscures mesothelial cell tracking. To overcome this limitation, we employed the PROCR transgenic mouse model in this experiment, ensuring more precise identification and analysis of pulmonary mesothelial cells.

A single dose of tamoxifen was administered to mice 3 days before the experiment to label a limited number of individual mesothelial cells. The bleomycin-induced IPF model was established as described in the Methods section, and organs were collected on days 0, 10, 14, and 28 for analysis (**Figure 5A**). **Figure 5B** shows trichrome staining results, revealing significant lung structural changes after bleomycin administration. Compared to controls, increased ECM deposition, thickened alveolar walls, and reduced airspaces were observed on days 10 and 14, confirming the successful establishment of the IPF model.

Mesothelial cells, typically characterized by their limited self-renewal capacity in adult tissues, display markedly distinct behavior in the context of IPF. In the bleomycin-induced IPF model, **Figure 5C** (left) quantifies the clonal

proliferation of mesothelial cells on the lung surface. Single-labeled mesothelial cells were observed to proliferate extensively, forming multicellular clones during the progression of fibrosis. The right panel of **Figure 5C** further classifies the proportions of clones by size, revealing a significant increase in multicellular clones on days 10 and 14, indicative of heightened mesothelial cell proliferating activity during this phase of the disease.

Cross sections in the central panel of **Figure 5C** provide additional evidence, demonstrating the formation of multilayered structures composed of proliferating mesothelial cells. This proliferative activity was corroborated through Ki67 immunostaining (**Figure 5D**), which marks actively proliferating cells. Together, these findings strongly suggest that mesothelial cells play a pivotal role in the fibrotic response during IPF, undergoing rapid proliferation to potentially contribute to tissue repair or fibrosis. Interestingly, by day 28 (**Figure 5C 5E**), the proliferative activity of mesothelial cells showed a marked decline, correlating with the resolution phase of the disease. This suggests that mesothelial cell proliferation is tightly regulated and temporally linked to the progression and subsequent repair phases of IPF. These observations underscore the dynamic and context-dependent nature of mesothelial cell behavior, highlighting their potential as key contributors to both the progression and resolution of fibrotic lung diseases.

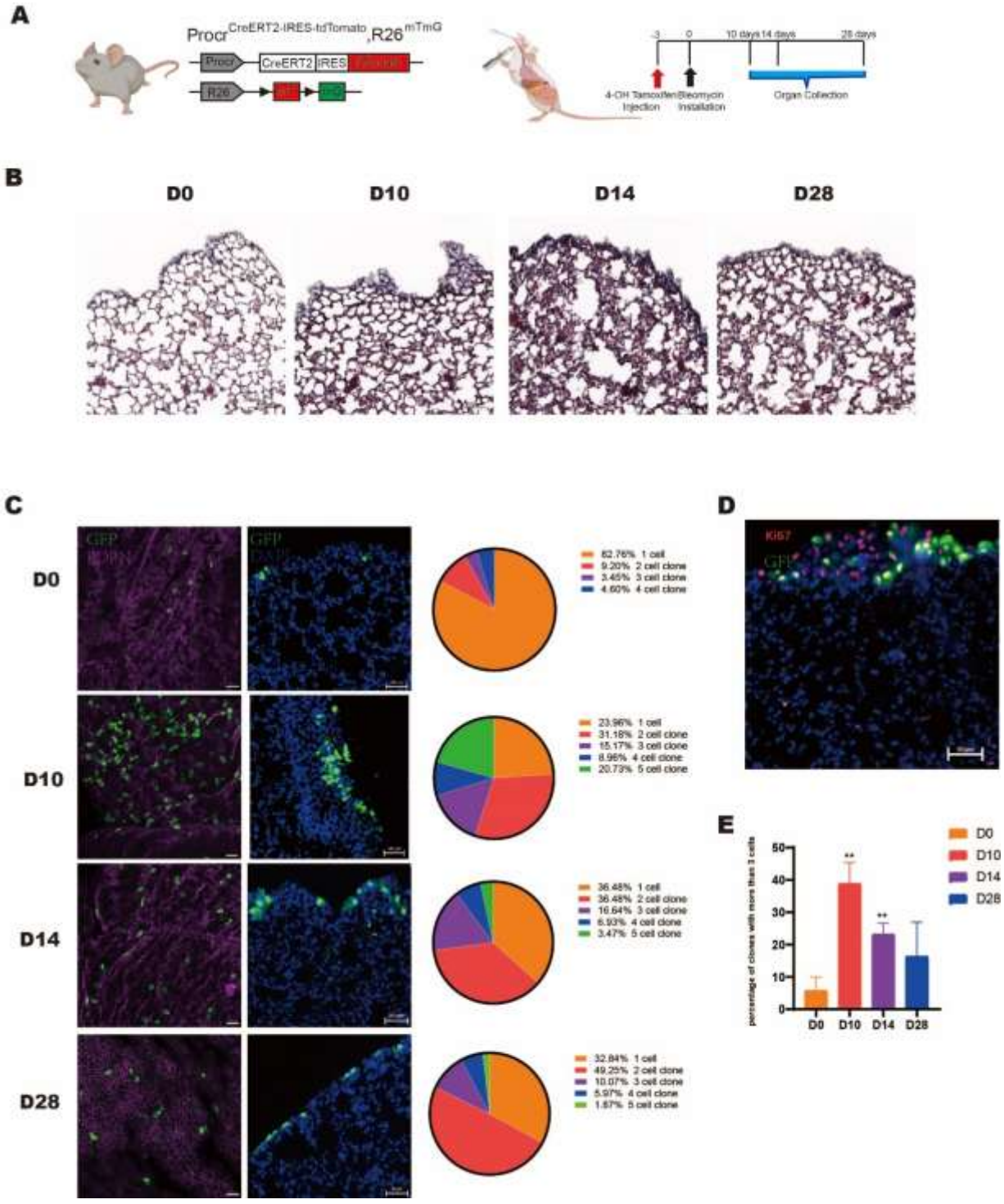

Figure 5: Proliferation of Mesothelial Cells on the Lung Surface in Bleomycin-Induced IPF Model (A) Overview of the experimental setup of the IPF model. (B) Masson's Trichrome Staining on Days 0, 10, 14, and 28 in Bleomycin-Induced IPF Model. (C) Lineage tracing results at days 0, 10, 14, and 28 in the bleomycin-induced IPF model. Left panel: Representative images of the lung surface,

showing GFP-labeled mesothelial cells (green), with PDPN immunofluorescence (magenta) and DAPI staining (blue). Middle panel: Lung tissue sections at each time point, visualized for mesothelial cell clones. Right panel: Proportional distribution of cells within clones of varying sizes. Scale bar=50 μm. (D) Lung sections at day 10 with Ki67 staining (red), indicating proliferating cells. Mesothelial cells are labeled with GFP (green). Scale bar=50 μm. (E) Statistics of mesothelial cell clones with over three cells on the lung surface in the IPF model. **$p \leq 0.01$. Two-tailed t-test.

3.4.2 Migration and Differentiation of Mesothelial Cells in IPF

In our study, we observed that mesothelial cells proliferate and form multicellular clones during the progression of IPF. This observation raises an important question: given that the mesothelium is a single-layered outer membrane, where do these proliferating cells go? To address this, we quantified mesothelial cells in multiple lung sections at various time points during IPF progression (**Figure 6A**). Using laminin, a basement membrane marker, we delineated the boundary between the lung surface and internal regions (**Figure 6B**). Cells external to the laminin-stained basement membrane were classified as "surface cells," while those internal to it were considered "internalized cells." Quantitative analysis revealed that the total number of mesothelial cells increased significantly by day 10 post-IPF induction, indicating active proliferation during this period. However, this proliferation plateaued in later stages, with no further substantial changes in the overall number of mesothelial cells as the disease progressed (**Figure 6E**). Interestingly, despite the lack of continued increase in cell numbers, a striking shift in their spatial distribution was observed. The proportion of mesothelial cells localized within the lung parenchyma increased steadily from D10 onward (**Figure 6C, F**), suggesting that mesothelial cells contribute to IPF not only by proliferating but also by migrating into the lung.

To further investigate whether the internalized mesothelial cells undergo differentiation into fibroblasts, we performed immunofluorescence staining on lung sections from IPF models at different time points (**Figure 6G**). Specifically, we used alpha-smooth muscle actin (α-SMA), a well-established fibroblast marker, alongside GFP for traced mesothelial cells. Our analysis revealed a progressive increase in the number of GFP/α-SMA double-positive cells over time, indicating that mesothelial cells were transitioning into fibroblasts. Moreover, we observed a notable shift in the spatial distribution of these cells,

with the initially surface-localized double-positive cells progressively migrating into deeper regions of the lung parenchyma as IPF advanced. This redistribution supports the hypothesis that mesothelial cells not only migrate but also undergo mesothelial-to-mesenchymal transition, subsequently differentiating into fibroblasts that contribute to the fibrotic remodeling characteristic of IPF.

In summary, during bleomycin-induced IPF, mesothelial cells exhibit a range of dynamic behaviors, including proliferation, migration, and differentiation. These cells actively respond to the fibrotic environment, migrating from the lung surface into the parenchyma and undergoing mesothelial-to-mesenchymal transition. This process contributes to the pool of fibroblasts involved in fibrotic remodeling. Additionally, mesothelial cells display region-specific adaptations, suggesting a meticulous role in IPF progression and underscoring their potential as targets for therapeutic intervention.

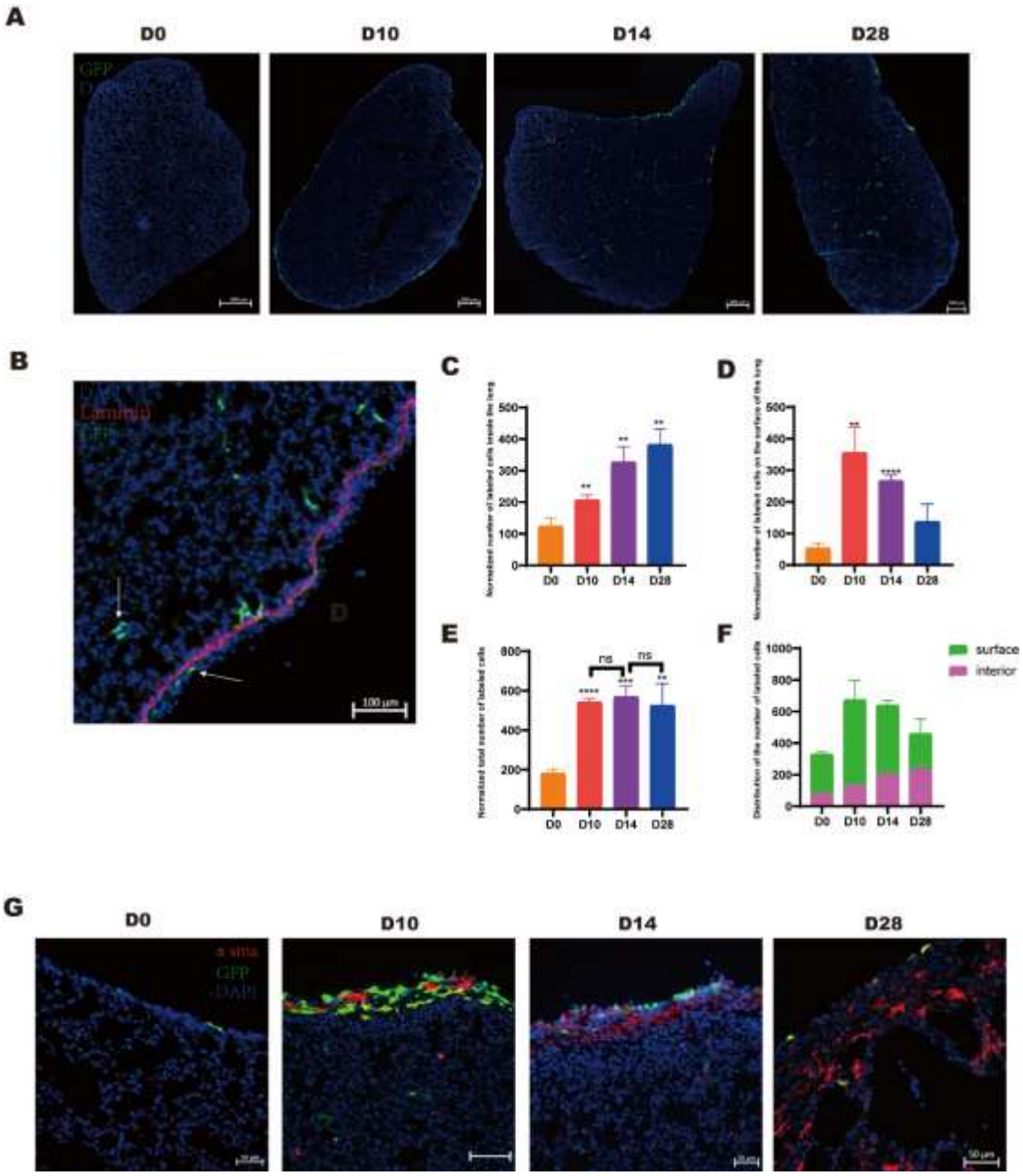

Figure 6: Mesothelial Cells Migrate and Differentiate During IPF Progression (A) Representative lung sections from an IPF model at D0, D10, D14, and D28, showing GFP-labeled mesothelial cells (green) and DAPI staining (blue) for cell nuclei. Scale bar=500 μm. (B) Representative immunofluorescence staining of lung sections showing laminin (red), GFP-labeled mesothelial cells (green), and DAPI-stained nuclei (blue). Arrows on the left and right indicate mesothelial cells located in the lung parenchyma (internal) and on the lung surface (external), respectively. Scale bar=100 μm. (C) Statistics of the number of normalized internal traced mesothelial cells in the IPF model. (D) Statistics of the number of normalized traced mesothelial cells on the surface of the lung. (E) Statistics of total number of traced mesothelial cells

in the IPF model. **p ≤ 0.01, ***p≤ 0.001, ****p≤ 0.0001. Two-tailed t-test. (F) Quantification of normalized labeled cells on the lung surface and within the lung parenchyma at different time points. (G) Representative immunofluorescence staining of lung sections from the IPF model at different time points, showing alpha-smooth muscle actin (α-SMA, red), traced mesothelial cells (green), and DAPI-stained nuclei (blue). Scale bar=50 μm.

3.5 Rapid Activation of Mesothelial Cells in Response to Injury

As we mentioned above, our study focused on elucidating the role of mesothelial cells in a pulmonary fibrosis model. As pulmonary fibrosis is a chronic disease with a protracted and complex progression, it is widely recognized that mesothelial cells may exhibit distinct and dynamic functions at various stages of the disease. To investigate these functional changes more directly and under controlled stress conditions, we designed a straightforward and highly specific experimental model.

In this model, we introduced a physical injury to the peritoneum of transgenic mice, creating an open-injury scenario. This approach allowed us to observe the immediate and localized responses of mesothelial cells to mechanical stress in a well-defined setting. The injured tissue was imaged directly under a microscope to capture high-resolution data on cellular behavior and morphological changes. **Figure 7A** provides a schematic representation of the experimental design. This approach offers valuable insights into the rapid activation and potential functional shifts of mesothelial cells in response to acute stress.

By live imaging tamoxifen-induced lineage-traced GFP+ mesothelial cells, we were able to visualize the dynamic changes occurring in mesothelial cells within 15 hours of injury, specifically in areas adjacent to the wound (**Figure 7B**). The left panel provides a low-magnification overview of the entire observed field, while the middle and right panels present magnified views of the specific regions outlined in the yellow and red boxes, respectively. At 0 hours post-injury, mesothelial cells retained their classic flattened cobblestone morphology characteristic of the steady-state condition, maintaining intact cell-cell connections. However, within 6 hours post-injury, both clusters of mesothelial cells in the observed regions displayed significant morphological and positional

changes. These changes included alterations in cell shape and shifts in cell positioning, indicative of an active response to the injury stimulus.

This rapid transformation reflects the highly dynamic nature of mesothelial cells under stress and highlights their capacity for swift adaptation to environmental changes. Such responsiveness suggests that mesothelial cells play an essential role in initiating and coordinating early tissue repair processes following injury.

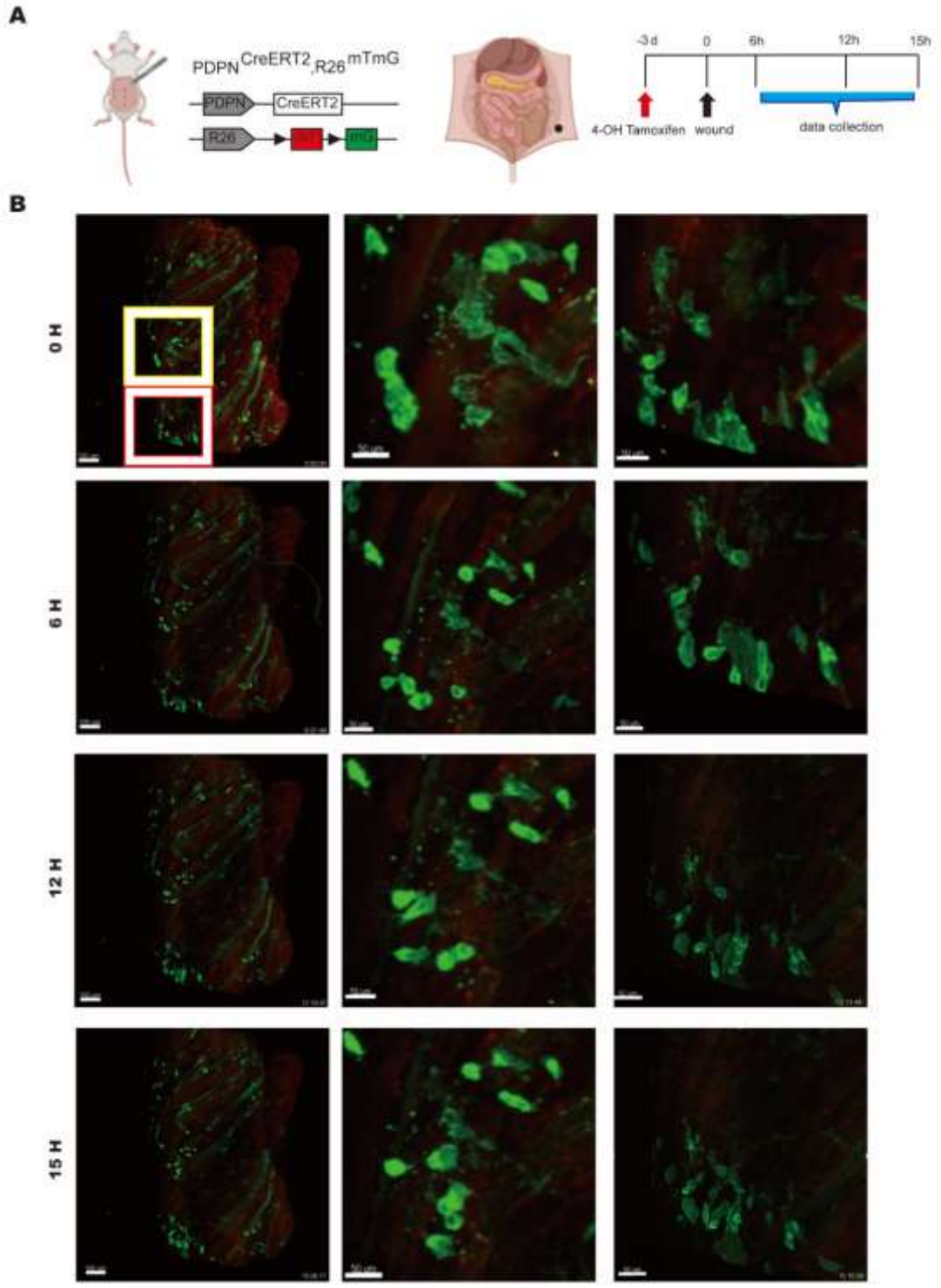

Figure 7: Dynamic changes in mesothelial cells observed within 15 hours of injury model (A) Overview of the experimental setup of the injury model. (B) Representative picture from the injury model at 0h, 6h, 12h, and 15h, showing GFP-labeled mesothelial cells (green) and td-tomato(red) for background. Left panel Scale bar=100 µm, middle panel and right panel Scale bar=50 µm

3.6 The Critical and Diverse Roles of Mesothelial Cells in Postoperative Adhesion Formation

3.6.1 Proliferation, Clonal Expansion, and Remodeling Roles of Mesothelial Cells in Postoperative Adhesions

In the previous sections, we explored the rapid morphological changes and migratory capacity of mesothelial cells in response to acute injury, highlighting their potential role in the early stages of surface wound repair. Building on these findings, we utilized a more complex postoperative adhesion model to investigate the diverse functions of mesothelial cells.

As a primary and critical step, we employed a tamoxifen-induced transgenic mouse model to trace mesothelial cell behavior, focusing specifically on clonal expansion within adhesion regions. **Figure 8A** provides an overview of the experimental design, illustrating the approach used to analyze mesothelial cell contributions to adhesion formation in this model. **Figure 8B** and **Figure 8C** display images of the adhesions and the corresponding Masson's trichrome staining results, respectively. In our optimized adhesion model, adhesions consistently form between the peritoneum and the cecum rather than involving other organs. This controlled formation enhances the reproducibility and reliability of the experimental setup, ensuring stable and consistent conditions for analysis.

By conducting surface tracing of GFP-labeled mesothelial cells alongside immunofluorescence staining for PDPN, we analyzed the adhesion regions to quantify the proportion of clones containing more than four cells on both the peritoneal and cecum sides (**Figure 8D**). The results demonstrate a marked increase in clonal expansion of mesothelial cells on both sides during adhesion formation. This clonal proliferation reflects an active response of mesothelial cells to the postoperative adhesion environment. Although mesothelial cells on both the peritoneal and cecum sides undergo significant proliferation and clonal expansion, proliferation on the peritoneal side is more pronounced at day 7. This suggests that the peritoneal side may experience a stronger or more immediate proliferative response, possibly due to differences in the local microenvironment or the mechanical properties of the tissue at the injury site. This disparity in proliferation could reflect the distinct roles and dynamics of

mesothelial cells in the process of adhesion formation and tissue repair.

To further validate these findings, we performed Ki67 staining on sections of the adhesion regions (**Figure 8E**). The staining results corroborated the presence of significant proliferative activity, confirming that mesothelial cells are not only actively involved in adhesion formation but also contribute to its progression through rapid and localized expansion. These observations highlight the pivotal role of mesothelial cells in the cellular dynamics of postoperative adhesions, suggesting that their proliferation and clonal expansion may be key processes driving adhesion development and stability.

It is well-known that in postoperative adhesion models, substantial adhesion bands can sometimes form between tissues or organs (**Figure 9A**). These bands are particularly challenging to resolve and represent a more severe form of adhesion. To investigate the role of mesothelial cells in such persistent adhesions, we performed 3D staining and imaging of D14 adhesion bands formed during the experiments. **Figure 9B** illustrates the distribution of GFP-labeled mesothelial cells (green), the basement membrane marker laminin (magenta), and the macrophage marker CD68 (red) within the adhesion band. A substantial number of GFP+ mesothelial cells are observed on the surface of the adhesion band. Based on our earlier findings, we infer that these mesothelial cells have undergone robust proliferation and migration, actively contributing to the formation of the adhesion band. Immunofluorescence staining for ASMA in the adhesion bands revealed the presence of a subset of GFP+ASMA+ mesothelial cells (**Figure 9D**). This indicates that some mesothelial cells may undergo differentiation into myofibroblast-like cells within the adhesion band, potentially contributing to the contractile properties and fibrotic remodeling of the adhesion structure. Unlike previous reports suggesting that macrophages primarily participate in the early stages of adhesion formation, our results indicate that macrophages also play a significant role in the development of adhesion bands This finding is further confirmed by MOMA-2 staining results shown in **Figure 9C**, which illustrate the significant presence and involvement of macrophages within the adhesion band. Interestingly, a nearly intact laminin layer is observed on the band surface, suggesting that as the adhesion matures, the surface of the band may eventually develop a normal mesothelial layer. This finding provides new insights into the dynamic remodeling of adhesion bands during their progression.

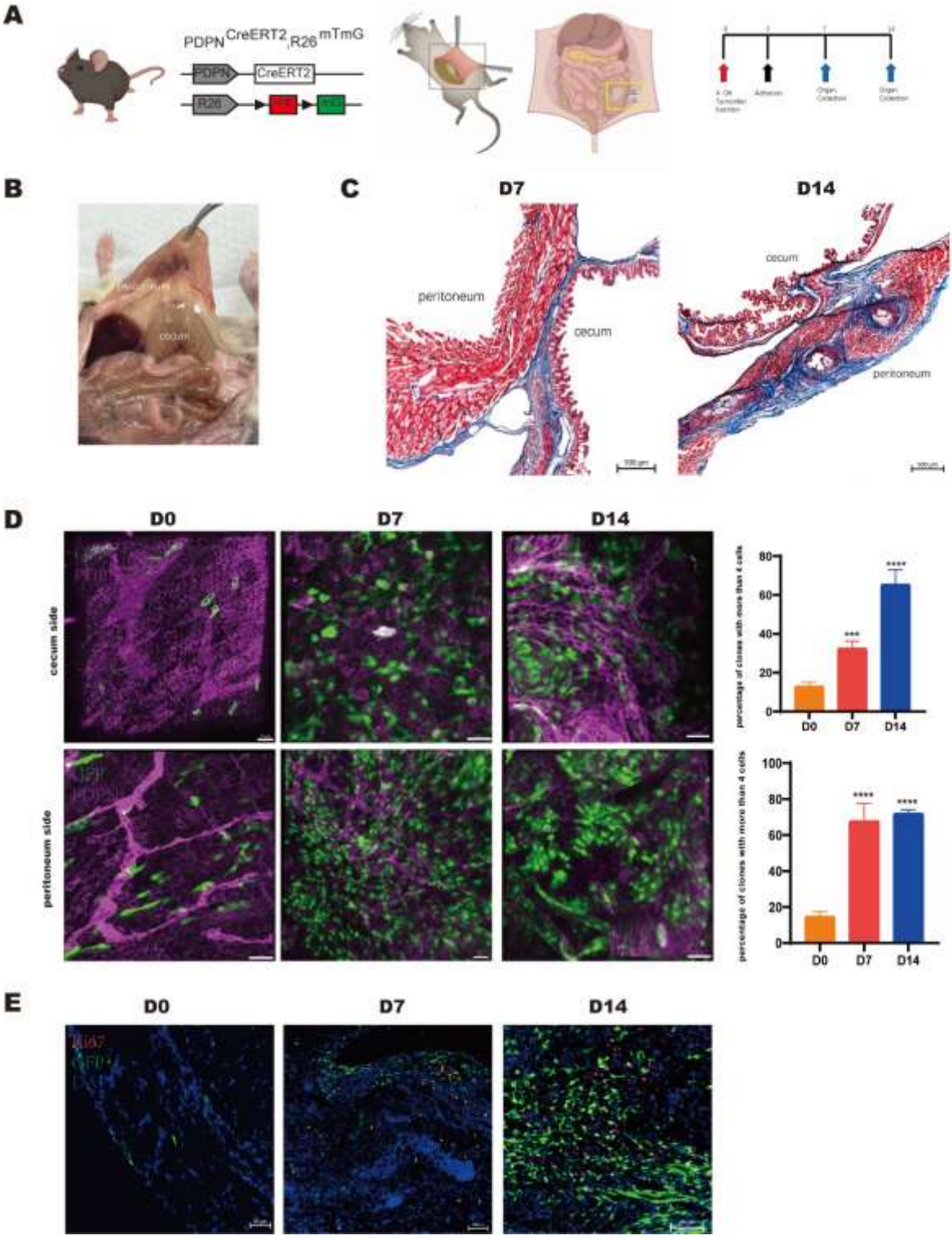

Figure 8: Proliferation and Clonal Expansion of Mesothelial Cells in Postoperative Adhesion Formation. (A) Experimental design of the postoperative adhesion model using tamoxifen-induced transgenic mice to trace mesothelial cell clonal expansion. (B) Representative images of adhesions formed between the peritoneum and cecum. (C) Masson's Trichrome Staining on Day 7 and D14 adhesion model. Scale bar=500 μm. (D) Representative images and statistics of

mesothelial cell clones with over four cells on the peritoneal and cecum sides of the adhesion regions, shown by GFP tracing and PDPN staining. Scale bar=50 μm. ***p≤ 0.001, ****p≤ 0.0001. Two-tailed t-test. (E) Representative images of Ki67 staining confirming mesothelial cell proliferation within the adhesion regions. Scale bar=50 μm.

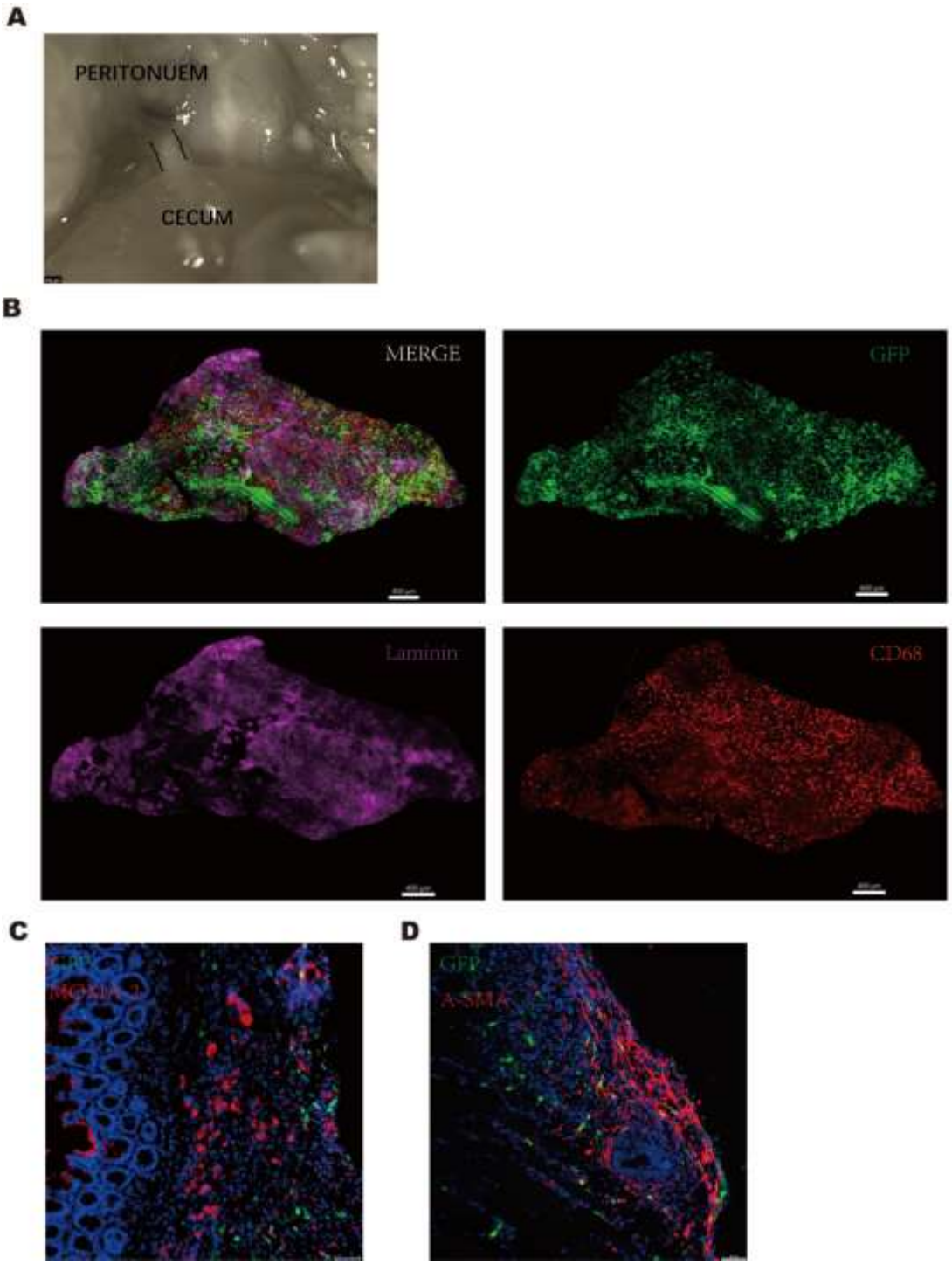

Figure 9: Spatial distribution of mesothelial cells and macrophages within the adhesion band. (A) Representative images of adhesion bands formed between

the peritoneum and cecum at day 14 post-surgery. Scale bar=200 μm. (B) 3D immunofluorescence staining of the adhesion band at day 14. The right upper panel shows GFP-labeled mesothelial cells (green), the left lower panel highlights laminin (magenta) distribution, and the right lower panel illustrates macrophages stained with CD68 (red). The left upper panel presents a merged image combining all markers. Scale bar=400 μm. (C) Representative images of MOMA-2 staining (red) within the adhesion band, showing the distribution of macrophages alongside GFP-labeled mesothelial cells (green) and nuclei stained with DAPI (blue). Scale bar=50 μm. (D) Representative images of ASMA staining (red) within the adhesion band, showing GFP-labeled mesothelial cells (green) and nuclei stained with DAPI (blue). Scale bar=50 μm.

3.6.2 Differentiated Mesothelial Cells in Myogenesis and Vascularization within Human and Mouse Adhesions

In the previous sections, we highlighted the robust proliferative activity of mesothelial cells and their potential differentiation into mesenchymal lineages during the progression of postoperative adhesions. Adhesion tissues, however, exhibit considerable heterogeneity in their composition and structure. Histological analysis of human adhesion tissues using Masson's trichrome staining revealed that the majority are primarily composed of collagen fibers, with minimal evidence of vascularization (**Figure 10A-B**).

In contrast, a subset of refractory adhesion tissues exhibited distinct features of myogenesis and vascularization, alongside a collagen-rich extracellular matrix (**Figure 10C-E**). These observations suggest that adhesion tissues undergo distinct remodeling processes, where mesothelial cells may contribute not only to collagen deposition but also to the formation of muscle-like and vascular structures in specific cases. The presence of myogenesis and vascularization in refractory adhesions implies a more complex and dynamic tissue remodeling environment, potentially influencing the persistence and severity of these adhesions.

To validate this hypothesis, we performed immunofluorescence staining for the endothelial cell marker CD31 in the D14 adhesion model of PDPN CreER mice (**Figure 10F-G**). The results showed no GFP+CD31+ mesothelial cells, indicating that mesothelial cells do not directly transdifferentiate into endothelial cells within the adhesion tissue. However, a subset of GFP+ mesothelial cells displayed spatial distribution consistent with pericyte-like characteristics. To further investigate this possibility, we conducted immunofluorescence staining

for the pericyte marker PDGFβ and the smooth muscle marker αSMA (**Figure 10H**). The findings revealed GFP+ PDGFβ+ cells in regions of myogenic differentiation within the adhesion tissue, suggesting that mesothelial cells may contribute to the vascular remodeling and myogenesis of adhesions by differentiating into pericytes-like cells. This supports the notion that mesothelial cells play a diverse and context-dependent role in adhesion formation.

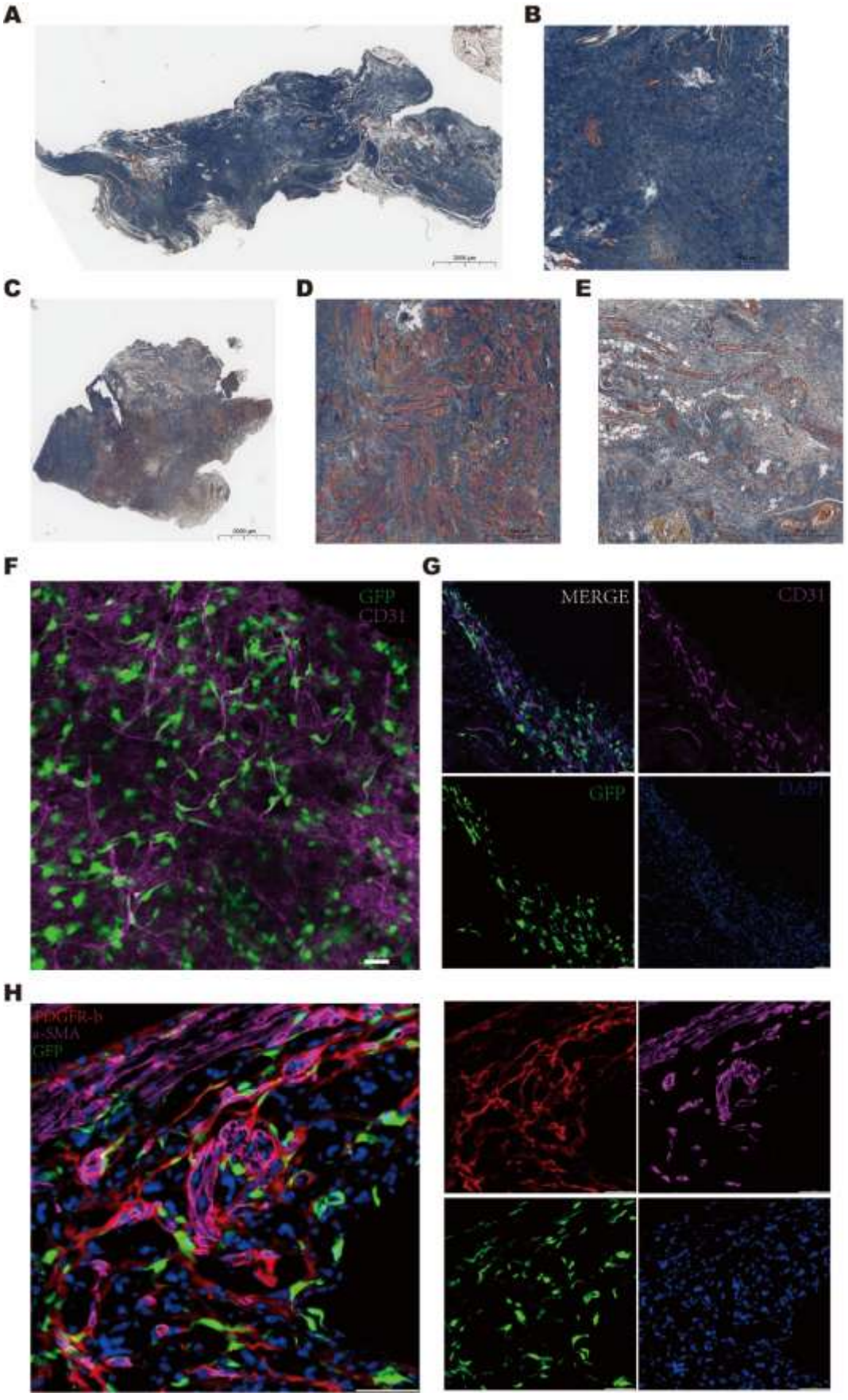
A
B
C
D
E
F
GFP
CD31
G
MERGE
CD31
GFP
H
PDGFR-b
a-SMA
GFP

Figure 10: Characterization of Mesothelial Cell in Human and Mouse Adhesion Tissues: Collagen Composition, Myogenesis, Vascularization, and Cellular Markers (A) Representative Masson's trichrome staining of human adhesion tissues showing collagen fiber-dominant adhesions with minimal vascularization. Scale bar=2000 μm. (B) High-magnification images of the collagen-dominant human adhesion tissue. Scale bar=200 μm. (C) Representative Masson's trichrome staining of human adhesion tissues displays features of myogenesis and vascularization alongside a collagen-rich extracellular matrix. Scale bar=2000 μm. (D) High-magnification images of human adhesion tissues with myogenic differentiation. Scale bar=500 μm. (E) High-magnification images of human adhesion tissues exhibiting neovascularization. Scale bar=500 μm. (F-G) Immunofluorescence staining for CD31 (magenta) and GFP-labeled mesothelial cells (green) in D14 $PDPN^{CreERT2}$ x $R26^{mTmG}$ mouse adhesion tissues. Scale bar=50 μm. (H)Immunofluorescence staining for the pericyte marker PDGFβ (red) and the smooth muscle marker αSMA (magenta) and nuclei stained with DAPI (blue) in $PDPN^{CreERT2}$ x $R26^{mTmG}$ mouse adhesion tissues. Scale bar=50 μm.

3.7 Exploring Mesothelial Cell Behavior in an Ex Vivo Culture Model.

In the preceding sections, we utilized various in vivo models combined with genetically modified mice to trace mesothelial cells and explore their functions or roles under different conditions. However, the limitations inherent to in vivo models—such as their complexity, ethical concerns, high costs, and difficulty in isolating specific cellular mechanisms—prompted us to turn to in vitro systems. In contrast, in vitro models offer significant advantages, including precise control of environmental conditions, ease of manipulation, reduced experimental complexity, and suitability for high-throughput analyses. To leverage these benefits, we established an ex vivo tissue culture model based on mouse peritoneum to further investigate the functional dynamics of mesothelial cells in a more controlled and accessible setting.

3.7.1 Mesothelial Cell Activation and Transition in an Ex Vivo Injury Model

We developed an ex vivo culture system using mouse peritoneum to study

mesothelial cell behavior. This model simulates surgical injury by applying gentle damage to the mesothelial layer with a cotton swab (**Figure 11A**). The primary advantage of this approach is its ability to isolate mesothelial cell responses from the complexities of the in vivo environment, allowing for a more targeted investigation into the cellular and molecular mechanisms underlying mesothelial reactions to trauma.

To investigate mesothelial cell behavior following injury, we performed 3D immunostaining for the mesothelial marker PDPN and the basement membrane marker laminin at different time points (**Figure 11B**). In the control group, the peritoneal mesothelial layer displayed a standard cobblestone-like morphology with intact cell-cell connections. Following localized injury, while the mesothelial cells were partially absent in the affected areas, their morphology remained unchanged. However, after 3 days of ex vivo culture, mesothelial cells exhibited striking morphological changes, including a loss of cell-cell junctions and a transition to a near-spherical shape. Notably, these morphological alterations were not observed in any in vivo models, underscoring the unique advantages of the ex vivo system for capturing distinct mesothelial cell responses to trauma. After 7 days in ex vivo culture, most of the mesothelial layer on the peritoneal surface had largely disappeared, with the remaining PDPN+ mesothelial cells predominantly migrating through the basement membrane into the underlying tissue. The differing changes observed in mesothelial cells between the ex vivo and in vivo injury models indicate that the regenerative and rapid migratory responses of mesothelial cells are probably influenced by the underlying tissue microenvironment and interactions with immune cells. In the ex vivo model, these factors are more controlled and isolated, which may limit the full spectrum of responses compared to the complex interactions present in the in vivo environment.

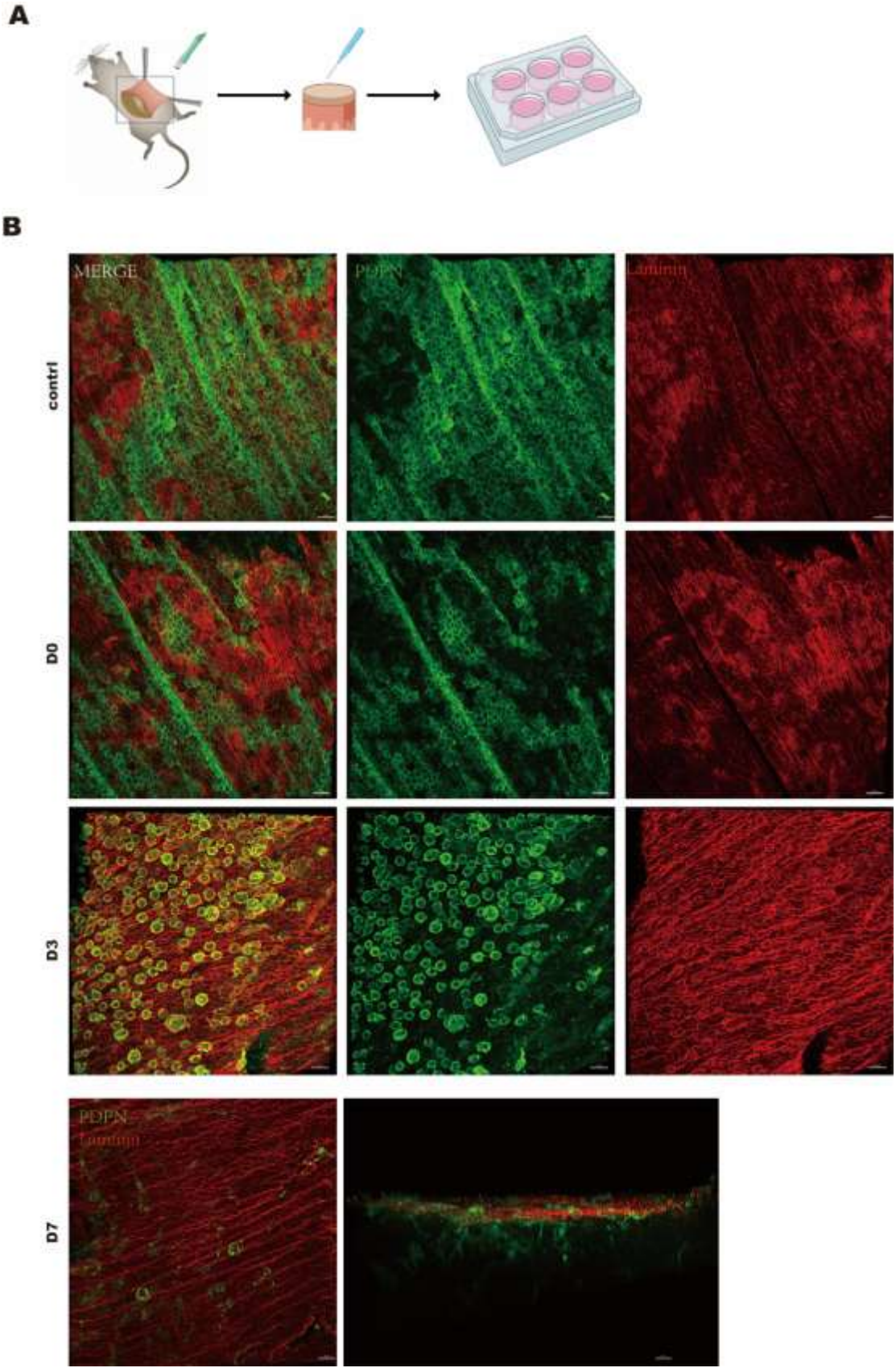

Figure 11: Ex Vivo Mesothelial Cell Behavior Following Injury. (A) Schematic of the experimental workflow demonstrating the setup for the ex vivo culture system

using mouse peritoneum. Gentle damage was applied to the mesothelial layer with a cotton swab to simulate surgical injury. (B) Time-course analysis of mesothelial cell responses following injury. 3D immunostaining for the mesothelial marker PDPN (green) and basement membrane marker laminin (red) was performed at different time points. Scale bar=30 μm.

3.7.2 Generation and Polarization of Macrophages Using the ER-Hoxb8 Cell Line

M1 and M2 macrophages are known to play distinct roles in tissue repair and inflammation in various diseases. We hypothesize that their interactions with mesothelial cells could significantly influence mesothelial cell activation following injury. To test this hypothesis, we explored how macrophage polarization (M1 or M2 phenotypes) modulates mesothelial cell behavior in an ex vivo injury model.

In this study, we utilized the ER-Hoxb8 cell line to generate polarized M1&M2 macrophages. **Figure 12A** outlines the differentiation process. For comparison, we also differentiated primary cells derived from mouse bone marrow into macrophages. **Figure 12B** illustrates the comparison between the ER-Hoxb8-derived cells and the bone marrow-derived cells in their differentiation into macrophages. Flow cytometry analysis (**Figure 12C**) demonstrates comparable differentiation efficiency between the two sources. Building on this, the differentiated macrophages were further polarized into M1 or M2 phenotypes. As shown in **Figure 12D**, flow cytometry analysis using established markers—CD80 for M1 macrophages and CD206 for M2 macrophages—demonstrates that ER-Hoxb8-derived macrophages can be successfully polarized into both M1 and M2 states. This validates the utility of this cell line for studying macrophage behavior, polarization, and functional interactions in our ex-vivo model.

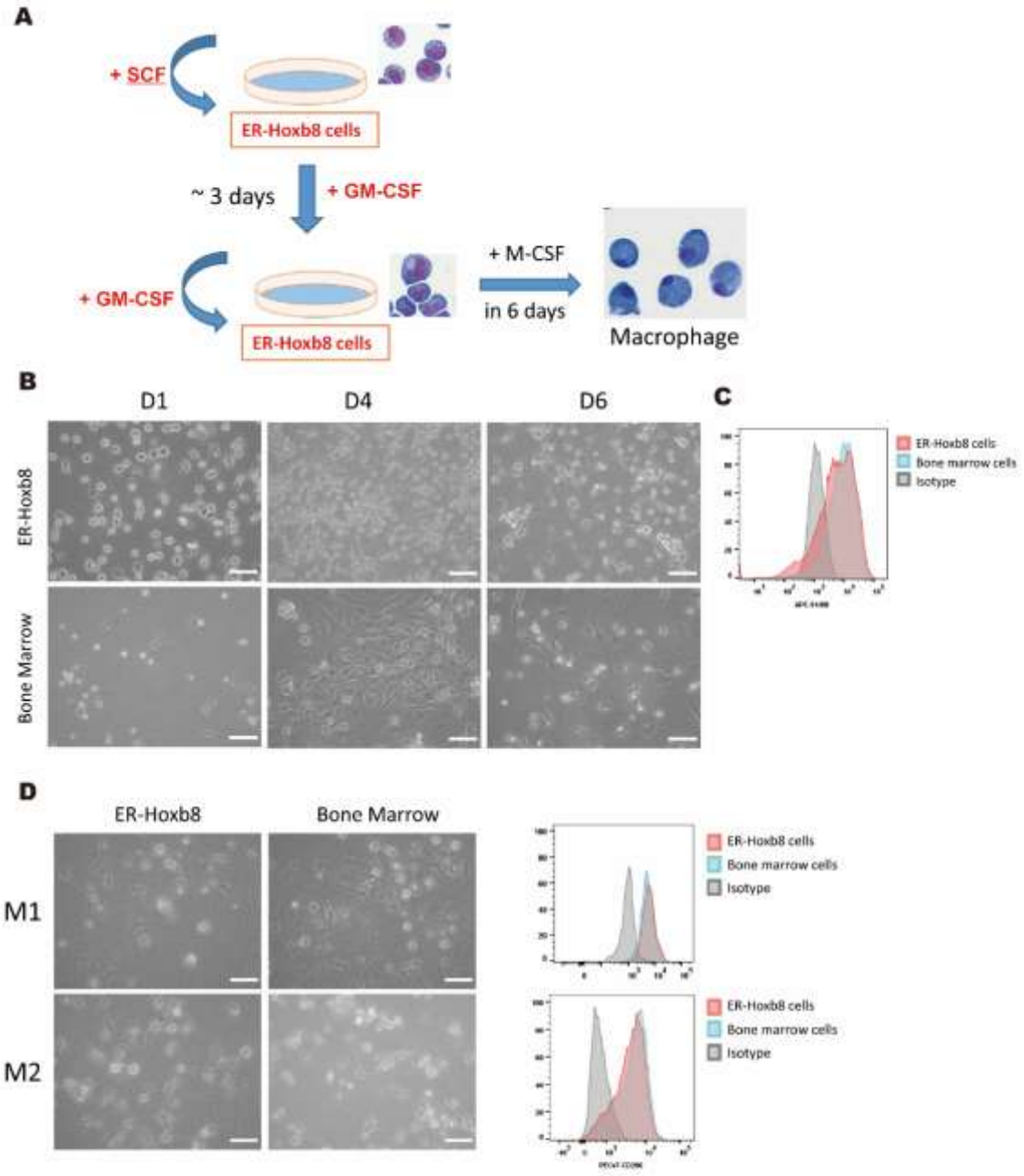

Figure 12: Generation and polarization of macrophages using the ER-Hoxb8 cell line. (A) Schematic representation of the differentiation process for ER-Hoxb8 cells into macrophages, followed by polarization into M1 or M2 phenotypes. (B) Comparative analysis of the differentiation potential of ER-Hoxb8 cells and mouse

bone marrow-derived cells into macrophages. Scale bar=50 µm. (C) Flow cytometry analysis showing comparable differentiation efficiency of ER-Hoxb8-derived cells and bone marrow-derived cells into macrophages. (D) Representative images of M1M2 polarization and flow cytometry results confirm successful polarization of ER-Hoxb8-derived macrophages into M1 and M2 phenotypes, using CD80 as a marker for M1 macrophages and CD206 for M2 macrophages. Scale bar=50 µm

3.7.3 M1 vs. M2 Macrophages: Impact on Mesothelial Activation and Migration

To investigate how polarized M1 and M2 macrophages influence mesothelial cell activation, we developed an ex vivo co-culture system using mouse peritoneum (**Figure 13A**). In the previously described injury model, mesothelial cells in isolation lose their intercellular junctions and adopt a near-spherical morphology after damage. Interestingly, when M1 macrophages were introduced into the co-culture system, mesothelial cells exhibited a pronounced activation response. Immunofluorescence staining for the mesothelial marker PDPN and the M1 macrophage marker CD80 showed clear evidence of mesothelial cell activation. (**Figure 13B**). Moreover, high-magnification images revealed close interactions between M1 macrophages and mesothelial cells that had not yet transitioned into an activated state (**Figure 13C**), suggesting direct macrophage involvement in initiating the activation process. Conversely, co-culture with M2 macrophages did not induce significant morphological or structural changes in mesothelial cells. The mesothelial layer retained its integrity, and cells appeared to maintain their original, quiescent state (**Figure 13D-E**). This finding indicates that M2 macrophages do not promote mesothelial cell activation and may instead contribute to preserving their resting phenotype.

By combining staining for the basement membrane marker laminin, we were able to analyze the relative spatial distribution of mesothelial cells. In co-culture with M1 macrophages, a portion of mesothelial cells was observed to no longer remain on the surface but instead migrate through the basement membrane and move deeper into the underlying tissue (**Figure 13F**). In contrast, in co-culture with M2 macrophages, this migration was not observed (**Figure 13G**).

These observations highlight the distinct roles of macrophage polarization states in regulating mesothelial cell behavior, with M1 macrophages acting as potent activators of mesothelial cells and M2 macrophages appearing to exert

a stabilizing effect. This differential influence reveals the importance of macrophage-mesothelial interactions in tissue repair and immune modulation.

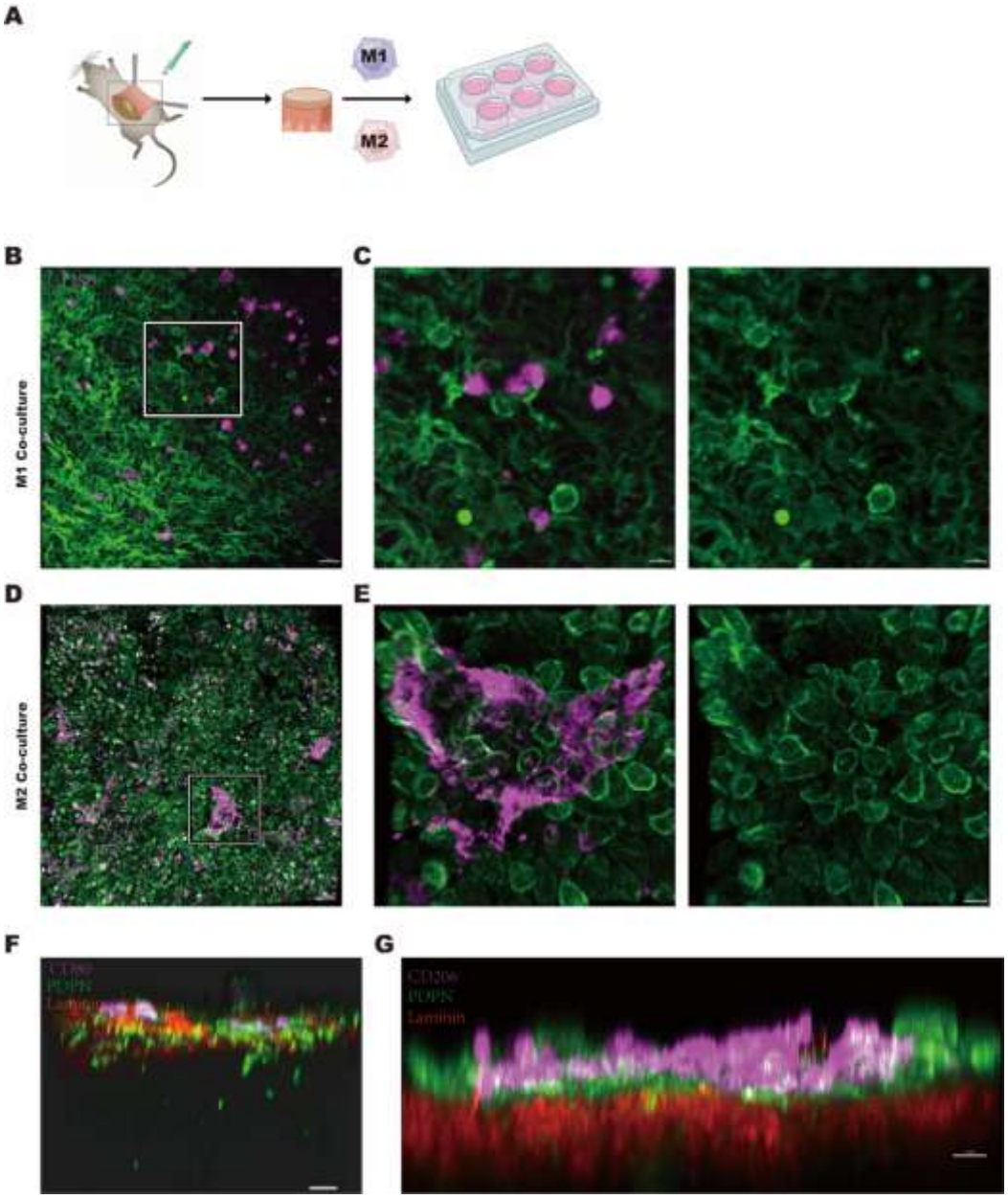

Figure 13: Distinct Effects of M1 and M2 Macrophages on Mesothelial Cell Activation and Migration in an Ex Vivo Co-Culture System (A) Schematic diagram of the mouse peritoneum co-culture system with polarized M1 or M2 macrophages. (B) 3D Immunofluorescence staining of mesothelial cells (PDPN, green) and M1 macrophages (CD80, magenta) shows mesothelial activation and morphological changes after co-culture with M1 macrophages. Scale bar=50 μm (C) High-magnification images highlight interactions between M1 macrophages and activated mesothelial cells. Scale bar=20 μm. (D) 3D Immunofluorescence staining of mesothelial cells (PDPN, green) and M2 macrophages (CD206, magenta) shows that M2 macrophages do not promote mesothelial cell activation. Scale bar=50 μm. (E)

High-magnification images highlight interactions between M2 macrophages and inactivated mesothelial cells. Scale bar=20 μm. (F) 3D immunofluorescence staining for the basement membrane marker laminin (red) and PDPN (green) demonstrates mesothelial cells migrating through the basement membrane after co-culture with M1 macrophages (CD80 magenta). Scale bars: 50 μm. (G) 3D immunofluorescence staining for laminin (red) and PDPN (green) shows no significant structural changes or migration observed in mesothelial cells during co-culture with M2 macrophages (CD206 magenta). Scale bars: 20 μm.

3.8 Utilizing Human-Derived Mesothelial Cells to Further Investigate Mesothelial Behavior

3.8.1 Isolation, Culture, and Injury Response of Human Mesothelial Cells.

To gain deeper insights into the properties and behavior of mesothelial cells, we tried to isolate and culture mesothelial cells from human tissue. The omentum, commonly available from abdominal surgeries, was chosen due to its accessibility, tissue abundance, and practicality for experimental purposes (**Figure 14A**). To investigate the spatial organization of mesothelial cells in human omental tissue, we performed 3D immunofluorescence staining combined with second harmonic generation imaging. The mesothelial cells were labeled using the mesothelial marker PDPN (red), while the collagen fibers within the tissue were visualized in green through the second harmonic generation (green). This analysis revealed that mesothelial cells are mostly located on the surface of fat lobules in the omentum (**Figure 14B-C**).

After continuous optimization of culture conditions, we successfully established an in vitro system for culturing human mesothelial cells. Under light microscopy, the isolated mesothelial cells demonstrated robust proliferative activity, forming colonies by day 7 and reaching confluency by day 14 (**Figure 14D**). This finding was further confirmed through Ki67 staining, which revealed significant proliferative activity of the cultured mesothelial cells (**Figure 14E**). These results indicate that the cultured mesothelial cells exhibit strong proliferative capacity and adaptability, validating the effectiveness of the culture system in providing a supportive microenvironment for mesothelial cell growth and expansion. After the mesothelial cells reached confluency, we simulated injury

by using a sharp instrument to create a physical scratch. Samples were collected and imaged 12 hours post-injury (**Figure 14F**). The results showed that mesothelial cells surrounding the damaged area exhibited notable morphological changes and actively migrated toward the injury site. Immunofluorescence staining for α-SMA indicated a significant presence of α-SMA+ cells in the damaged area, suggesting that the repair process involves not only cell migration but also mesothelial-to-mesenchymal transition.

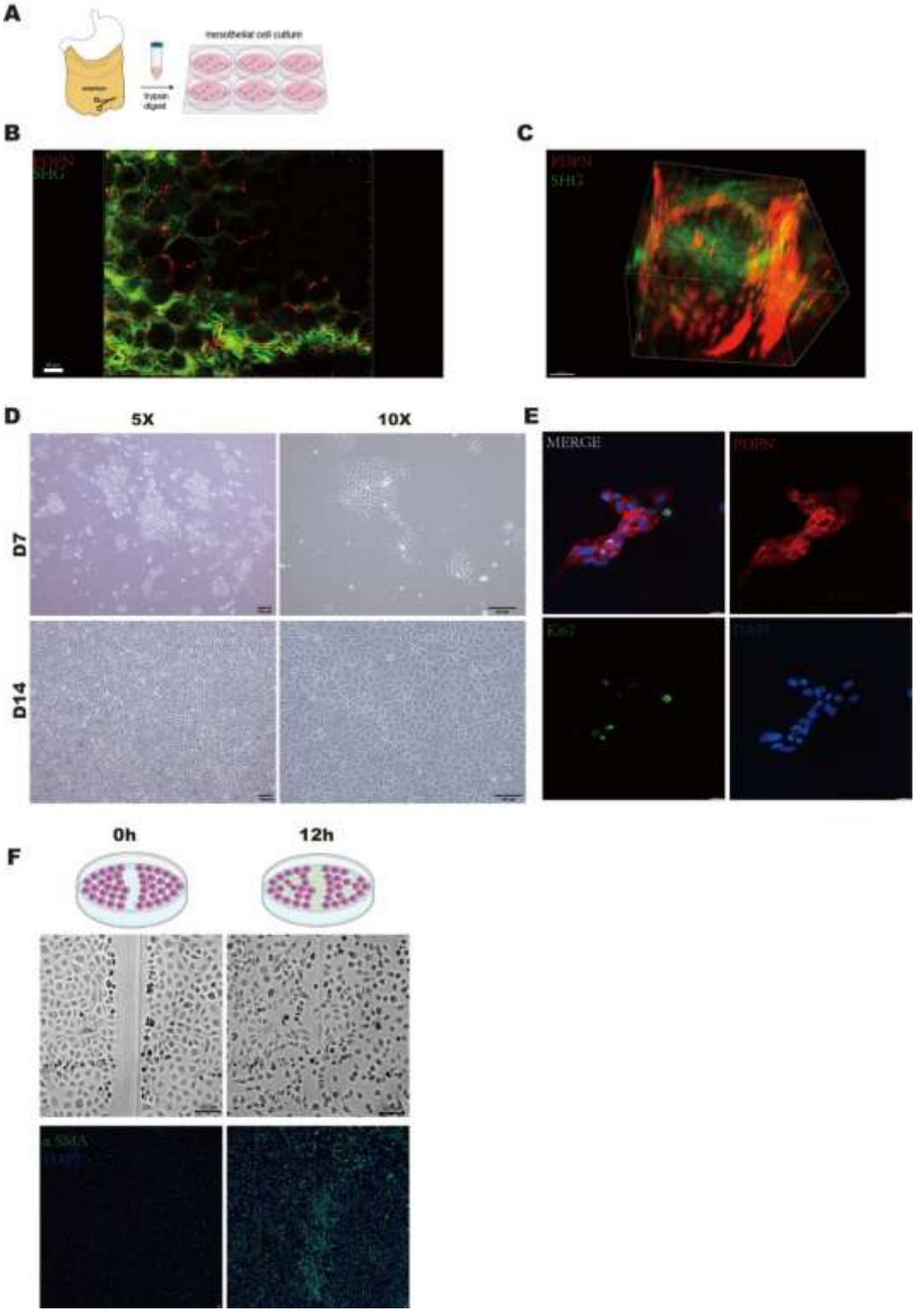

Figure 14: Human mesothelial cell isolation, culture, and response to injury. (A) Schematic of the isolation process of mesothelial cells from human omentum obtained during abdominal surgery. (B-C) Spatial organization of mesothelial cells in the omentum, visualized by 3D immunofluorescence staining for PDPN (red)

and second harmonic generation imaging for collagen fibers (green), highlighting mesothelial cells on the surface of fat lobules. Scale bars: 50 μm. (D) Light microscopy images of mesothelial cells, forming colonies by day 7 and reaching confluency by day 14. Scale bar: 100 μm. (E) Immunofluorescence staining for PDPN (red) Ki67(green) demonstrates significant proliferative activity of cultured human mesothelial cells. Scale bar: 20 μm. (F) Injury response was simulated by creating a scratch on the mesothelial monolayer, followed by imaging 12 hours post-injury. α-SMA (green) immunofluorescence staining indicates the presence of α-SMA+ cells in the injury area. Scale bar: 100 μm.

3.8.2 TGF-β1 Induces Mesothelial-to-Mesenchymal Transition and Cytoskeletal Remodeling in Cultured Human Mesothelial Cells

TGF-β1 is a key regulator of matrix protein deposition and fibrosis, with its role implicated in various disease models. To investigate its effects on mesothelial cells, we treated near-confluent cultured human mesothelial cells with 10 ng/ml of TGF-β1. Changes in cell morphology were documented using light microscopy over 12 hours (**Figure 15A**). In the control group, mesothelial cells maintained their characteristic cobblestone-like morphology with minimal changes, whereas in the TGF-β1-treated group, significant morphological alterations were observed, suggesting a mesothelial-to-mesenchymal transition.

These changes were further validated using α-SMA immunofluorescence and phalloidin staining for the cytoskeleton, both of which demonstrated increased cytoskeletal remodeling and stress fiber formation in TGF-β1-treated cells (**Figure 15C**). To quantify these morphological changes, we used ImageJ software for cell segmentation and analyzed parameters such as circularity and area (**Figures 15B, 15D-E**). The analysis revealed a significant decrease in circularity and an increase in cell area in the TGF-β1-treated group compared to the control. This indicates that TGF-β1 induces a transition to a more elongated and spread-out phenotype.

These findings highlight the ability of TGF-β1 to drive cytoskeletal remodeling and promote MMT in mesothelial cells, potentially contributing to pathological conditions such as fibrosis and adhesion formation. Furthermore, this study establishes a robust model for investigating the cellular and molecular mechanisms of TGF-β1-induced changes in mesothelial cell behavior,

providing insights into therapeutic strategies targeting TGF-β1-related pathways.

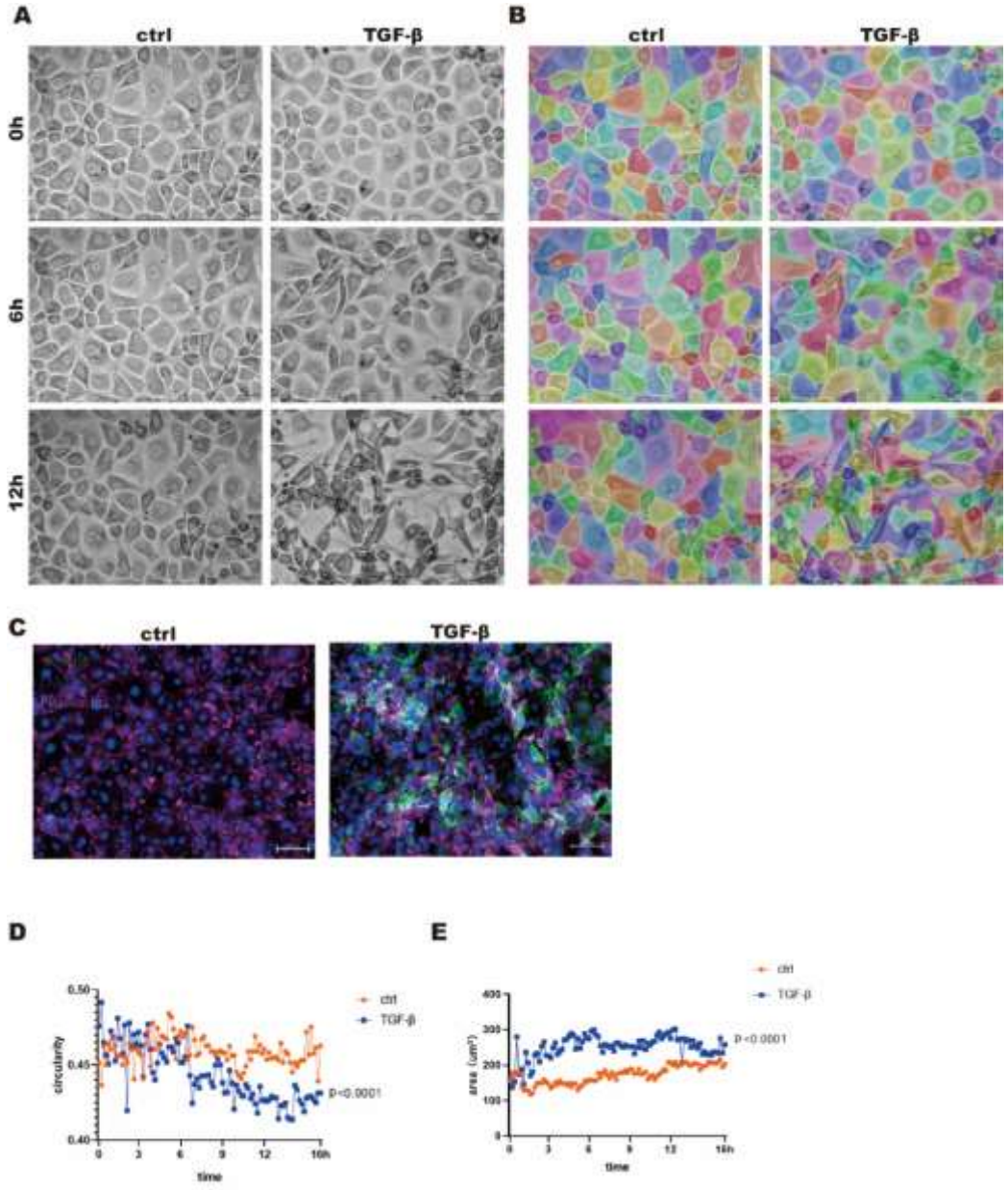

Figure 15: TGF-β1 induces morphological changes and mesothelial-to-mesenchymal transition (MMT) in cultured human mesothelial cells. (A) Brightfield microscopy images showing the morphological changes of mesothelial cells over 12 hours with or without 10 ng/mL TGF-β1 treatment. Scale bar: 20 µm. (B) Cell segmentation analysis using ImageJ software to quantify morphological differences. Representative segmented images illustrate alterations in cell shape after TGF-β1 treatment. Scale bar: 20 µm. (C) Immunofluorescence staining for α-SMA (green) and phalloidin (magenta) reveals cytoskeletal remodeling and increased α-SMA expression in TGF-β1-treated cells, further confirming MMT. DAPI (blue) stains nuclei. Scale bar: 100 µm. (D-E) Quantitative analysis of cell morphology using

circularity and area measurements. TGF-β1 treatment significantly decreases circularity (D) and increases cell area (E), reflecting the transition to an elongated and mesenchymal-like phenotype. Paired t-test $p \leq 0.0001$.

4 Discussion

Mesothelial cells (MCs) are critical players in various physiological and pathological processes. This study provides an integrative exploration of mesothelial cell dynamics across diverse contexts. In this study, we utilized inducible PDPN^{CreERT2} and ProCr^{CreER} transgenic mouse models to investigate mesothelial cell clonality across various stages, including aging, postnatal development, and injury. This study provides an integrative exploration of mesothelial cell dynamics across diverse contexts, utilizing both in vivo and ex vivo models to investigate their proliferation, migration, and functional characteristics.

Mesothelial cells exhibit remarkable proliferative activity during early organ development. Embryonic mesothelial cells can transform into mesenchymal cells, which contribute to the connective, vascular, and organ-specific tissues of developing organs [99]. In our study, neonatal mice, clonal expansion of mesothelial cells on organ surfaces, particularly the lung, underscores their role in shaping organ architecture. Excessive proliferation in this phase appears to be tightly regulated to ensure proper organ morphogenesis and function. RNA sequencing analyses during this developmental phase revealed significant upregulation of genes associated with cell cycle progression and matrix remodeling, providing insights into the molecular mechanisms driving mesothelial proliferation. This rapid proliferation phase contrasts with the restricted replicative capacity during adult homeostasis, in which mesothelial cells remain primarily in a quiescent state. During homeostasis, mesothelial cells maintain their epithelial phenotype, ensuring structural integrity and barrier function of serosal surfaces.

In pathological states such as Idiopathic pulmonary fibrosis (IPF), mesothelial cells transition to a mesenchymal phenotype, contributing to extracellular matrix deposition and fibrosis progression. Liu et al. demonstrated that bleomycin-induced pleural mesothelial cells (PMCs) migrate into the lung parenchyma and localize near lung fibroblasts in the subpleural area. In vitro, they found that PMCs promote fibroblast transformation into myofibroblasts, while fibroblasts induce PMCs to undergo mesothelial-mesenchymal transition (MMT). Their findings suggest that TGF-β1 signaling plays a key role in this interaction, as its inhibition reduces collagen-I expression and attenuates pulmonary fibrosis. Additionally, they reported activation of the Wnt/β-catenin signaling pathway during PMC and fibroblast crosstalk [101].These findings align with previous

studies identifying mesothelial cells as progenitors for stromal lineages, further cementing their role in organ remodeling and pathological conditions. Injury models also highlight the rapid activation of mesothelial cells, exhibiting morphological and functional changes indicative of EMT. In our ex vivo injury model, mesothelial cells lost cell-cell junctions and adopted a more migratory phenotype. This activation was further confirmed through increased expression of α-SMA and remodeling of the actin cytoskeleton. Mesothelial cells are highly responsive to localized damage, migrating to injury sites and contributing to tissue repair. However, these reparative processes often involve pathological MMT, predisposing tissues to fibrosis and adhesion formation. Postoperative adhesions present another pathological context for mesothelial cell behavior. Our data show that mesothelial cells proliferate and undergo clonal expansion during adhesion formation, contributing to vascularization and myogenesis within adhesion tissues. This dual role both reparative and pathological underscores the complexity of mesothelial cell functions in adhesion biology. The transition to myofibroblasts and other stromal cell types via MMT further highlights their involvement in fibrotic remodeling.

In fibrosis, adhesion, and injury models, macrophages play a well-established role in disease progression. Their phenotype and function can be influenced by various factors, shaping their impact on pathological processes. In the study of the relationship between mesothelial cells and macrophages, the most well-known research focuses on the field of ovarian cancer. In ovarian cancer metastasis, macrophages contribute by promoting the adhesion of ovarian cancer cells to mesothelial cells. This occurs through the induction of adhesion-related gene expression in mesothelial cells. Key regulators of this process include ITGA2, VEGFC, and the JNK and Akt pathways, which enhance the adhesion of macrophage-stimulated mesothelial cells to ovarian cancer cells [102].

Furthermore, studies have demonstrated that macrophage polarization significantly affects mesothelial cells. Traditionally, macrophages are classified into two main polarization states: M1 and M2. Both play critical roles in inflammatory processes, with M1 macrophages primarily mediating pro-inflammatory responses, while M2 macrophages are predominantly associated with anti-inflammatory functions [103]. Earlier studies suggest a link between macrophages and the EMT of peritoneal mesothelial cells (PMCs). Shi et al. found that co-culturing PMCs with M1 macrophages induced EMT-like changes, including reduced E-cadherin and increased α-SMA expression, while M2

macrophages had no significant effect [104]. However, a contrasting study showed that EMT markers were upregulated in PMCs co-cultured with M1, M2a, and M2c macrophages, with M2c having the strongest effect, suggesting a more prominent role for M2c in promoting EMT [105].In our study, the role of macrophages in modulating mesothelial responses was explored through tissue co-culture system. We found that macrophages play a crucial role in regulating mesothelial cell responses, with M1 and M2 macrophages exhibiting distinct effects. M1 macrophages promote mesothelial activation, inducing enhanced migration, morphological changes, and upregulation of α-SMA, which are hallmarks of a profibrotic response. In contrast, M2 macrophages exert minimal influence on mesothelial cell morphology and migration, suggesting a less pronounced role in driving mesothelial activation. These differential effects indicate that macrophage polarization significantly impacts mesothelial-mediated processes, particularly in fibrosis and adhesion formation.

The most common approach for studying mesothelial cells relies on in vitro culture systems. However, these systems are often limited by spontaneous differentiation or contamination with fibroblasts, making it difficult to conduct rigorous studies. Our optimized culture system effectively overcomes these challenges, allowing mesothelial cells to maintain their characteristic properties. Notably, the cells exhibit classic cobblestone-like colony growth, providing a more reliable and controlled model for studying mesothelial cell behavior and this system provides a physiologically relevant model for investigating mesothelial cell biology under controlled conditions. The cultured cells exhibited a robust proliferative capacity, forming distinct colonies within 7 days and reaching full confluency by day 14, while maintaining their characteristic cobblestone-like morphology. These features confirm their mesothelial identity and demonstrate their suitability for long-term in vitro studies.

This platform enabled detailed investigations into mesothelial cell dynamics, including their response to various physiological and pathological stimuli, such as injury, inflammatory signals, and growth factor stimulation. Among these, TGF-β1 emerged as a potent regulator of mesothelial cell behavior. Exposure to TGF-β1 induced a mesothelial-to-mesenchymal transition, characterized by upregulated α-SMA expression, cytoskeletal reorganization, and a shift from cobblestone-like to spindle-shaped morphology. These changes are hallmarks of a profibrotic response and are associated with pathological conditions such as peritoneal fibrosis and adhesion formation. More importantly, this in vitro system not only advances our understanding of mesothelial cell function and

pathology but also lays a crucial foundation for future applications in drug testing, therapeutic development, regenerative medicine, and tissue engineering. By providing a reliable platform for screening antifibrotic agents, investigating mesothelial cell repair mechanisms, and optimizing bioengineered tissue constructs, this model has the potential to drive significant advancements in the treatment of mesothelial-related diseases.

The findings from this study provide critical insights into the multifaceted roles of mesothelial cells in development, homeostasis, and pathological conditions. The observed dynamic transitions, particularly in response to injury and inflammatory signals, underscore the plasticity of mesothelial cells and their potential as therapeutic targets in fibrosis and adhesion prevention. Future studies should aim to elucidate the molecular pathways driving mesothelial activation and EMT, investigate the interplay between mesothelial cells and immune cell subsets under different inflammatory conditions, and explore pharmacological interventions to modulate TGF-β1 signaling and mesothelial EMT in clinical settings. By bridging developmental biology, immunology, and regenerative medicine, this research lays the foundation for novel strategies to mitigate peritoneal injury and adhesion-related complications while harnessing the regenerative potential of mesothelial cells for therapeutic applications.

5 Reference

1. MUTSAERS, S.E., *Mesothelial cells: Their structure, function and role in serosal repair.* Respirology, 2002. **7**(3): p. 171-191.
2. Koopmans, T. and Y. Rinkevich, *Mesothelial to mesenchyme transition as a major developmental and pathological player in trunk organs and their cavities.* Communications Biology, 2018. **1**(1): p. 170.
3. Rinkevich, Y., et al., *Identification and prospective isolation of a mesothelial precursor lineage giving rise to smooth muscle cells and fibroblasts for mammalian internal organs, and their vasculature.* Nat Cell Biol, 2012. **14**(12): p. 1251-60.
4. Fischer, A., et al., *Post-surgical adhesions are triggered by calcium-dependent membrane bridges between mesothelial surfaces.* Nature Communications, 2020. **11**(1): p. 3068.
5. Kawanishi, K., *Diverse properties of the mesothelial cells in health and disease.* Pleura and Peritoneum, 2016. **1**: p. 79 - 89.
6. Mutsaers, S.E., et al., *Mesothelial cells and peritoneal homeostasis.* Fertility and Sterility, 2016. **106**(5): p. 1018-1024.
7. Mutsaers, S.E., *The mesothelial cell.* The International Journal of Biochemistry & Cell Biology, 2004. **36**(1): p. 9-16.
8. Mutsaers, S.E., et al., *Mesothelial cells in tissue repair and fibrosis.* Front Pharmacol, 2015. **6**: p. 113.
9. Yung, S. and T.M. Chan, *Pathophysiological Changes to the Peritoneal Membrane during PD-Related Peritonitis: The Role of Mesothelial Cells.* Mediators of Inflammation, 2012. **2012**(1): p. 484167.
10. Hall*, J.C., et al., *The pathobiology of peritonitis.* Gastroenterology, 1998. **114**(1): p. 185-196.
11. Betjes, M.G.H., et al., *Interleukin-8 Production by Human Peritoneal Mesothelial Cells in Response to Tumor Necrosis Factor-α, Interleukln-1, and Medium Conditioned by Macrophages Cocultured with Staphylococcus epidermidis.* The Journal of Infectious Diseases, 1993. **168**(5): p. 1202-1210.
12. Li, F.K., et al., *Leukocyte migration across human peritoneal mesothelial cells is dependent on directed chemokine secretion and ICAM-1 expression.* Kidney International, 1998. **54**(6): p. 2170-2183.
13. Bittinger, F., et al., *PECAM-1 Expression in Human Mesothelial Cells: An in vitro Study.* Pathobiology, 2008. **64**(6): p. 320-327.
14. Lee, S.K., et al., *Exogenous Nitric Oxide Inhibits VCAM-1 Expression in Human Peritoneal Mesothelial Cells: Role of Cyclic GMP and NF-κB.* Nephron, 2002. **90**(4): p. 447-454.
15. Müller, J. and T. Yoshida, *Interaction of Murine Peritoneal Leukocytes and Mesothelial Cells: In Vitro Model System to Survey Cellular Events on Serosal Membranes during Inflammation.* Clinical Immunology and Immunopathology, 1995. **75**(3): p. 231-238.
16. Bellingan, G., et al., *In vivo fate of the inflammatory macrophage during the resolution of inflammation: inflammatory macrophages do not die locally, but emigrate to the draining lymph nodes.* Journal of immunology, 1996. **157 6**: p. 2577-85.

17. Bellingan , G.J., et al., *Adhesion Molecule–dependent Mechanisms Regulate the Rate of Macrophage Clearance During the Resolution of Peritoneal Inflammation.* Journal of Experimental Medicine, 2002. **196**(11): p. 1515-1521.
18. Yung, S. and T.M. Chan, *Intrinsic cells: mesothelial cells -- central players in regulating inflammation and resolution.* Perit Dial Int, 2009. **29 Suppl 2**: p. S21-7.
19. Yung, S. and T.M. Chan, *Hyaluronan--regulator and initiator of peritoneal inflammation and remodeling.* Int J Artif Organs, 2007. **30**(6): p. 477-83.
20. Topley, N., et al., *Human peritoneal mesothelial cell prostaglandin synthesis: induction of cyclooxygenase mRNA by peritoneal macrophage-derived cytokines.* Kidney Int, 1994. **46**(3): p. 900-9.
21. Kumar, A., et al., *Expression and assembly of procoagulant complexes by human pleural mesothelial cells.* Thromb Haemost, 1994. **71**(5): p. 587-92.
22. Ivarsson, M.L., et al., *Characterization and fibrinolytic properties of mesothelial cells isolated from peritoneal lavage.* Scand J Clin Lab Invest, 1998. **58**(3): p. 195-203.
23. Shetty, S., et al., *Urokinase receptor in human malignant mesothelioma cells: role in tumor cell mitogenesis and proteolysis.* Am J Physiol, 1995. **268**(6 Pt 1): p. L972-82.
24. Mutsaers, S.E., D. Whitaker, and J.M. Papadimitriou, *Stimulation of Mesothelial Cell Proliferation by Exudate Macrophages Enhances Serosal Wound Healing in a Murine Model.* The American Journal of Pathology, 2002. **160**(2): p. 681-692.
25. Livingston, E.M., *A clinical study of the abdominal cavity and peritoneum: Tenth installment.* The American Journal of Surgery, 1930. **10**(1): p. 417-472.
26. Raftery, A.T., *Regeneration of parietal and visceral peritoneum: an enzyme histochemical study.* Journal of anatomy, 1976. **121**(Pt 3): p. 589-597.
27. Foley-Comer, A.J., et al., *Evidence for incorporation of free-floating mesothelial cells as a mechanism of serosal healing.* J Cell Sci, 2002. **115**(Pt 7): p. 1383-9.
28. Cameron, G.R., S.M. Hassan, and S.N. De, *Repair of Glisson's capsule after tangential wounds of the liver.* The Journal of Pathology and Bacteriology, 1957. **73**: p. 1-10.
29. Ryan, G.B., J. Grobéty, and G. Majno, *Mesothelial injury and recovery.* Am J Pathol, 1973. **71**(1): p. 93-112.
30. Wheeldon, E.B., A.T. Mariassy, and K.D. McSporran, *The pleura: a combined light microscopic and scanning and transmission electron microscopic study in the sheep. II. Response to injury.* Exp Lung Res, 1983. **5**(2): p. 125-40.
31. Chen, K.S., et al., *Potential role of bone marrow-derived cells in the turnover of mesothelium.* Ren Fail, 2010. **32**(9): p. 1081-7.
32. Teranishi, S., M. Sakaguchi, and H. Itaya, *Mesothelial regeneration in the rat and effect of urokinase.* Nihon Geka Hokan, 1977. **46**(4): p. 361-79.
33. Tolhurst Cleaver, C.L., et al., *The effect of postoperative peritoneal lavage on survival, peritoneal wound healing and adhesion formation following fecal peritonitis: an experimental study in the rat.* Br J Surg, 1974. **61**(8): p. 601-4.
34. Hekking, L.H.P., et al., *Mesothelial Cell Transplantation in Models of Acute Inflammation and Chronic Peritoneal Dialysis.* Peritoneal Dialysis International, 2003. **23**(4): p. 323-330.
35. Wilm, B., et al., *The serosal mesothelium is a major source of smooth muscle cells of the gut vasculature.* Development, 2005. **132**(23): p. 5317-28.

36. Cai, C.-L., et al., *A myocardial lineage derives from Tbx18 epicardial cells.* Nature, 2008. **454**(7200): p. 104-108.
37. Que, J., et al., *Mesothelium contributes to vascular smooth muscle and mesenchyme during lung development.* Proc Natl Acad Sci U S A, 2008. **105**(43): p. 16626-30.
38. Dixit, R., X. Ai, and A. Fine, *Derivation of lung mesenchymal lineages from the fetal mesothelium requires hedgehog signaling for mesothelial cell entry.* Development, 2013. **140**(21): p. 4398-406.
39. Nasreen, N., et al., *Pleural mesothelial cell transformation into myofibroblasts and haptotactic migration in response to TGF-beta1 in vitro.* Am J Physiol Lung Cell Mol Physiol, 2009. **297**(1): p. L115-24.
40. Yang, A.H., J.Y. Chen, and J.K. Lin, *Myofibroblastic conversion of mesothelial cells.* Kidney Int, 2003. **63**(4): p. 1530-9.
41. Patel, P., et al., *Platelet derived growth factor B and epithelial mesenchymal transition of peritoneal mesothelial cells.* Matrix Biol, 2010. **29**(2): p. 97-106.
42. Liu, Q., et al., *Transforming growth factor {beta}1 induces epithelial-mesenchymal transition by activating the JNK-Smad3 pathway in rat peritoneal mesothelial cells.* Perit Dial Int, 2008. **28 Suppl 3**: p. S88-95.
43. Strippoli, R., et al., *Epithelial-to-mesenchymal transition of peritoneal mesothelial cells is regulated by an ERK/NF-kappaB/Snail1 pathway.* Dis Model Mech, 2008. **1**(4-5): p. 264-74.
44. Rennard, S.I., et al., *Role of pleural mesothelial cells in the production of the submesothelial connective tissue matrix of lung.* Am Rev Respir Dis, 1984. **130**(2): p. 267-74.
45. Laurent, P., et al., *Quantitation of elastin in human urine and rat pleural mesothelial cell matrix by a sensitive avidin-biotin ELISA for desmosine.* J Immunol Methods, 1988. **107**(1): p. 1-11.
46. Milligan, S.A., et al., *Characterization of proteoglycans produced by rat pleural mesothelial cells in vitro.* Exp Lung Res, 1995. **21**(4): p. 559-75.
47. Xiao, L., et al., *Connective tissue growth factor knockdown attenuated matrix protein production and vascular endothelial growth factor expression induced by transforming growth factor-beta1 in cultured human peritoneal mesothelial cells.* Ther Apher Dial, 2010. **14**(1): p. 27-34.
48. Ma, C., R.W. Tarnuzzer, and N. Chegini, *Expression of matrix metalloproteinases and tissue inhibitor of matrix metalloproteinases in mesothelial cells and their regulation by transforming growth factor-beta1.* Wound Repair Regen, 1999. **7**(6): p. 477-85.
49. Perfumo, F., et al., *Effects of peritoneal effluents on mesothelial cells in culture: cell proliferation and extracellular matrix regulation.* Nephrol Dial Transplant, 1996. **11**(9): p. 1803-9.
50. Owens, M.W. and S.R. Grimes, *Pleural mesothelial cell response to inflammation: tumor necrosis factor-induced mitogenesis and collagen synthesis.* Am J Physiol, 1993. **265**(4 Pt 1): p. L382-8.
51. Zhang, H., et al., *Effect of TGF-β1 Stimulation on the Smad Signal Transduction Pathway of Human Peritoneal Mesothelial Cells.* Int J Biomed Sci, 2005. **1**(1): p. 8-15.

52. Van der Meeren, A., et al., *Effect of epidermal growth factor on rat pleural mesothelial cell growth.* J Cell Physiol, 1990. **144**(1): p. 137-43.
53. Kimura, N. and I. Kimura, *Podoplanin as a marker for mesothelioma.* Pathol Int, 2005. **55**(2): p. 83-6.
54. Giri, H., I. Biswas, and A.R. Rezaie, *Activated protein C inhibits mesothelial-to-mesenchymal transition in experimental peritoneal fibrosis.* J Thromb Haemost, 2023. **21**(1): p. 133-144.
55. Isaksson, K., et al., *Long-term follow-up for adhesive small bowel obstruction after open versus laparoscopic surgery for suspected appendicitis.* Ann Surg, 2014. **259**(6): p. 1173-7.
56. Alonso Jde, M., et al., *Peritoneal response to abdominal surgery: the role of equine abdominal adhesions and current prophylactic strategies.* Vet Med Int, 2014. **2014**: p. 279730.
57. Ito, T., et al., *Cell barrier function of resident peritoneal macrophages in post-operative adhesions.* Nature Communications, 2021. **12**(1): p. 2232.
58. Lee, J.H., et al., *Tissue anti-adhesion potential of ibuprofen-loaded PLLA–PEG diblock copolymer films.* Biomaterials, 2005. **26**(6): p. 671-678.
59. Kement, M., et al., *Heparin for adhesion prevention: comparison of three different dosages with Seprafilm in a murine model.* Int J Surg, 2011. **9**(3): p. 225-8.
60. Irkorucu, O., et al., *Reduction of postsurgical adhesions in a rat model: a comparative study.* Clinics (Sao Paulo), 2009. **64**(2): p. 143-8.
61. Takazawa, R., et al., *Mesothelial cell sheets cultured on fibrin gel prevent adhesion formation in an intestinal hernia model.* Tissue Eng, 2005. **11**(3-4): p. 618-25.
62. Asano, T., et al., *Transplantation of an autologous mesothelial cell sheet prepared from tunica vaginalis prevents post-operative adhesions in a canine model.* Tissue Eng, 2006. **12**(9): p. 2629-37.
63. Brochhausen, C., et al., *Current strategies and future perspectives for intraperitoneal adhesion prevention.* J Gastrointest Surg, 2012. **16**(6): p. 1256-74.
64. Mutsaers, S.E., et al., *Mesothelial cells in tissue repair and fibrosis.* Frontiers in Pharmacology, 2015. **6**.
65. Massagué, J., *TGFbeta signaling: receptors, transducers, and Mad proteins.* Cell, 1996. **85**(7): p. 947-50.
66. Lee, Y.C., et al., *Transforming growth factor-beta induces collagen synthesis without inducing IL-8 production in mesothelial cells.* Eur Respir J, 2003. **22**(2): p. 197-202.
67. Hadjicharalambous, M.R. and M.A. Lindsay, *Idiopathic Pulmonary Fibrosis: Pathogenesis and the Emerging Role of Long Non-Coding RNAs.* Int J Mol Sci, 2020. **21**(2).
68. Sgalla, G., et al., *Idiopathic pulmonary fibrosis: pathogenesis and management.* Respir Res, 2018. **19**(1): p. 32.
69. Raghu, G., et al., *An official ATS/ERS/JRS/ALAT statement: idiopathic pulmonary fibrosis: evidence-based guidelines for diagnosis and management.* Am J Respir Crit Care Med, 2011. **183**(6): p. 788-824.
70. Richeldi, L., et al., *Efficacy and Safety of Nintedanib in Idiopathic Pulmonary Fibrosis.* New England Journal of Medicine, 2014. **370**(22): p. 2071-2082.

71. Habiel, D.M. and C.M. Hogaboam, *Heterogeneity of Fibroblasts and Myofibroblasts in Pulmonary Fibrosis.* Current Pathobiology Reports, 2017. **5**(2): p. 101-110.
72. Raghu, G., et al., *Incidence and prevalence of idiopathic pulmonary fibrosis.* American journal of respiratory and critical care medicine, 2006. **174**(7): p. 810-816.
73. Hung, C., et al., *Role of lung pericytes and resident fibroblasts in the pathogenesis of pulmonary fibrosis.* American journal of respiratory and critical care medicine, 2013. **188**(7): p. 820-830.
74. Nasreen, N., et al., *Pleural mesothelial cell transformation into myofibroblasts and haptotactic migration in response to TGF-β1 in vitro.* American Journal of Physiology-Lung Cellular and Molecular Physiology, 2009. **297**(1): p. L115-L124.
75. Karki, S., et al., *Wilms' tumor 1 (Wt1) regulates pleural mesothelial cell plasticity and transition into myofibroblasts in idiopathic pulmonary fibrosis.* The FASEB Journal, 2014. **28**(3): p. 1122.
76. Song, L.-J., et al., *Lethal (2) giant larvae regulates pleural mesothelial cell polarity in pleural fibrosis.* Biochimica et Biophysica Acta (BBA)-Molecular Cell Research, 2018. **1865**(9): p. 1201-1210.
77. Chen, L.-J., et al., *Bleomycin induced epithelial–mesenchymal transition (EMT) in pleural mesothelial cells.* Toxicology and applied pharmacology, 2015. **283**(2): p. 75-82.
78. Devuyst, O., P.J. Margetts, and N. Topley, *The pathophysiology of the peritoneal membrane.* J Am Soc Nephrol, 2010. **21**(7): p. 1077-85.
79. Selgas, R., et al., *Functional longevity of the human peritoneum: how long is continuous peritoneal dialysis possible? Results of a prospective medium long-term study.* Am J Kidney Dis, 1994. **23**(1): p. 64-73.
80. Margetts, P.J. and P. Bonniaud, *Basic mechanisms and clinical implications of peritoneal fibrosis.* Perit Dial Int, 2003. **23**(6): p. 530-41.
81. Williams, J.D., et al., *Morphologic changes in the peritoneal membrane of patients with renal disease.* J Am Soc Nephrol, 2002. **13**(2): p. 470-479.
82. Plum, J., et al., *Peritoneal sclerosis in peritoneal dialysis patients related to dialysis settings and peritoneal transport properties.* Kidney International, 2001. **59**: p. S42-S47.
83. Mateijsen, M.A., et al., *Vascular and interstitial changes in the peritoneum of CAPD patients with peritoneal sclerosis.* Perit Dial Int, 1999. **19**(6): p. 517-25.
84. Yoshida, E., et al., *Modulation of the receptor for urokinase-type plasminogen activator in macrophage-like U937 cells by inflammatory mediators.* Inflammation, 1996. **20**: p. 319-326.
85. Kim, J.-J., et al., *High glucose decreases collagenase expression and increases TIMP expression in cultured human peritoneal mesothelial cells.* Nephrology Dialysis Transplantation, 2008. **23**(2): p. 534-541.
86. McLoughlin, R.M., et al., *Differential regulation of neutrophil-activating chemokines by IL-6 and its soluble receptor isoforms.* The Journal of Immunology, 2004. **172**(9): p. 5676-5683.
87. Tomino, Y., *Mechanisms and interventions in peritoneal fibrosis.* Clinical and experimental nephrology, 2012. **16**: p. 109-114.
88. Haslinger, B., et al., *Simvastatin suppresses tissue factor expression and increases*

fibrinolytic activity in tumor necrosis factor-α–activated human peritoneal mesothelial cells. Kidney international, 2003. **63**(6): p. 2065-2074.

89. Di Paolo, N., et al., *Autologous peritoneal mesothelial cell implant in rabbits and peritoneal dialysis patients.* Nephron, 1991. **57**(3): p. 323-331.
90. Yung, S., et al., *Emodin ameliorates glucose-induced morphologic abnormalities and synthesis of transforming growth factor β1 and fibronectin by human peritoneal mesothelial cells.* Peritoneal dialysis international, 2001. **21**(3_suppl): p. 41-47.
91. Zhang, L., et al., *Fluvastatin inhibits the expression of fibronectin in human peritoneal mesothelial cells induced by high-glucose peritoneal dialysis solution via SGK1 pathway.* Clinical and experimental nephrology, 2015. **19**: p. 336-342.
92. Lee, Y.-C., et al., *Shorter daily dwelling time in peritoneal dialysis attenuates the epithelial-to-mesenchymal transition of mesothelial cells.* BMC nephrology, 2014. **15**: p. 1-9.
93. Sandoval, P., et al., *Carcinoma-associated fibroblasts derive from mesothelial cells via mesothelial-to-mesenchymal transition in peritoneal metastasis.* J Pathol, 2013. **231**(4): p. 517-31.
94. Siu, M.K.Y., et al., *PDK1 promotes ovarian cancer metastasis by modulating tumor-mesothelial adhesion, invasion, and angiogenesis via α5β1 integrin and JNK/IL-8 signaling.* Oncogenesis, 2020. **9**(2): p. 24.
95. Yasui, H., et al., *CCL2 secreted from cancer-associated mesothelial cells promotes peritoneal metastasis of ovarian cancer cells through the P38-MAPK pathway.* Clin Exp Metastasis, 2020. **37**(1): p. 145-158.
96. Ren, J., et al., *Lysophosphatidic acid is constitutively produced by human peritoneal mesothelial cells and enhances adhesion, migration, and invasion of ovarian cancer cells.* Cancer Res, 2006. **66**(6): p. 3006-14.
97. Natarajan, S., et al., *Collagen Remodeling in the Hypoxic Tumor-Mesothelial Niche Promotes Ovarian Cancer Metastasis.* Cancer Res, 2019. **79**(9): p. 2271-2284.
98. Bridda, A., et al., *Peritoneal mesothelioma: a review.* MedGenMed, 2007. **9**(2): p. 32.
99. Broeckx, G. and P. Pauwels, *Malignant peritoneal mesothelioma: a review.* Translational Lung Cancer Research, 2018. **7**(5): p. 537-542.
100. Nemec, K.M., et al., *Microglia replacement by ER-Hoxb8 conditionally immortalized macrophages provides insight into Aicardi-Goutières Syndrome neuropathology*. 2025, eLife Sciences Publications, Ltd.
101. Liu, F., et al., *Crosstalk between pleural mesothelial cell and lung fibroblast contributes to pulmonary fibrosis*. Biochimica et Biophysica Acta (BBA) - Molecular Cell Research, 2020. **1867**(11): p. 118806.
102. Cho, S.K., et al., *Macrophages Promote Ovarian Cancer-Mesothelial Cell Adhesion by Upregulation of ITGA2 and VEGFC in Mesothelial Cells.* Cells, 2023. **12**(3).
103. Yunna, C., et al., *Macrophage M1/M2 polarization.* European Journal of Pharmacology, 2020. **877**: p. 173090.
104. Shi, J., et al., *The Role of TLR4 in M1 Macrophage-Induced Epithelial-Mesenchymal Transition of Peritoneal Mesothelial Cells.* Cell Physiol Biochem, 2016. **40**(6): p. 1538-1548.
105. Tian, L., et al., *Epithelial-mesenchymal Transition of Peritoneal Mesothelial Cells Is Enhanced by M2c Macrophage Polarization.* Immunol Invest, 2022. **51**(2): p. 301-315.

6 Acknowledgements

The past four years have passed in the blink of an eye, and as I write this, I am overwhelmed by a sense of unreality. Looking back on my PhD journey, I find it filled with moments of regret and helplessness—times beyond my control and outcomes that left me with deep sighs. Yet, amidst the uncertainties and disappointments, there were also scattered moments of joy, glimmers of warmth, and gratitude that deserve to be acknowledged and remembered.

Above all, I am most grateful to my parents and my wife. As the most important people in my life, their unwavering support and boundless understanding have made this achievement possible—without them, I may not have even started on this path.

I am also deeply thankful to my supervisor, Dr. Yuval Rinkevich, he always encouraged me to explore freely. I was never criticized for pursuing bold, unconventional ideas, even when, in hindsight, some of my experiments were driven by nothing more than wishful thinking. I am truly grateful for the freedom he granted me in the lab and for the respect he showed toward my ideas. Moreover, I am also deeply grateful to my TAC members, Prof. Dr. Jürgen Behr and Prof. Markus Rehberg, for their feedback and suggestions on my research and thesis.

To my brother, Haifeng—you are, in every sense, a good man, someone who has fought tirelessly to change his own destiny. It has been my privilege to know you. Now that you have back to China to establish your own lab and are soon to be married, I sincerely wish you all the best in this new chapter of your life.

Aydan and Andy, my closest friends—your countless acts of kindness, both in the lab and in life, have meant the world to me. Together, we have shared hundreds, perhaps even thousands, of coffee breaks (and cigarette breaks) in Munich’s gray afternoons. For some reason, I feel that these moments will be among the flashes of memory that revisit me in my final moments.

Jiakuan and Chris—two colleagues I deeply admire. With your sharp minds and distinctive personalities, our discussions always left me feeling slightly inadequate, but only because you both constantly came up with such brilliant ideas.

To the many other colleagues who have been part of this journey—I won’t name

each of you individually, as you may prefer not to be mentioned, but please know that I wish you all success and fulfillment in your paths.

As I reach the end of this acknowledgment, I am acutely aware of the limits of my own words. I only hope that ChatGPT has managed to refine my thoughts into something worthy of the gratitude I feel and that these late-night reflections, written with teary eyes, have not been in vain.

7 Affidavit

LMU LUDWIG-MAXIMILIANS-UNIVERSITÄT MÜNCHEN

Dean's Office Medical Faculty
Faculty of Medicine

Affidavit

su, yiqun

Surname, first name

I hereby declare, that the submitted thesis entitled

Mesothelial Cell Plasticity and Function: Insights from In Vivo Lineage Tracing, Injury Models, and Human-Derived Cell Studies

is my own work. I have only used the sources indicated and have not made unauthorised use of services of a third party. Where the work of others has been quoted or reproduced, the source is always given.

I further declare that the dissertation presented here has not been submitted in the same or similar form to any other institution for the purpose of obtaining an academic degree.

Munich 21.03.2025

Place, Date

Yiqun Su

Signature doctoral candidate

Affidavit PhD Medical Research

Date: 21.03.2025

8 Confirmation of Congruency

LMU LUDWIG-MAXIMILIANS-UNIVERSITÄT MÜNCHEN

Dean's Office Medical Faculty
Doctoral Office

Confirmation of congruency between printed and electronic version of the doctoral thesis

su, yiqun

Surname, first name

I hereby declare that the electronic version of the submitted thesis, entitled

Mesothelial Cell Plasticity and Function: Insights from In Vivo Lineage Tracing, Injury Models, and Human-Derived Cell Studies

is congruent with the printed version both in content and format.

Munich 21.03.2025

Place, Date

Yiqun Su

Signature doctoral candidate

Congruency of submitted versions PhD Medical Research

Date: 21.03.2025

9 List of Publications

1. Fischer A, Han W, Hu S, Mück-Häusl M, Wannemacher J, Kadri S, Lin Y, Dai R, Christ S, **Su Y**, Dasgupta B, Sardogan A, Deisenhofer C, Dutta S, Kadri A, Gü ney TG, Correa-Gallegos D, Mayr CH, Hatz R, Stoleriu MG, Lindner M, Hilgendorff A, Adler H, Machens HG, Schiller HB, Hauck SM, Rinkevich Y. Targeting pleuro-alveolar junctions reverses lung fibrosis in mice. Nat Commun. 2025 Jan 2;16(1):173. doi: 10.1038/s41467-024-55596-x. Erratum in: Nat Commun. 2025 Feb 24;16(1):1911. doi: 10.1038/s41467-025-57261-3. PMID: 39747171; PMCID: PMC11696612.

2. Aydan Sardogan, **Yiqun Su** et al, Yuval Rinkevich, "Clonal analysis of mesothelium" (manuscript under preparation)